Comparison of Iced Aerodynamic Measurements on a Swept Wing from Two Wind Tunnels

Sam Lee[*]
Vantage Partners, LLC, Cleveland, Ohio, 44135 USA

Andy Broeren[†]
NASA John H. Glenn Research Center, Cleveland, Ohio, 44135 USA

Brian S. Woodard[‡]
University of Illinois at Urbana-Champaign, Urbana, Illinois, 61801 USA

Christopher W. Lum[§]
University of Washington, Seattle, Washington, 98195 USA

and

Timothy G. Smith[**]
FAA William J. Hughes Technical Center, Atlantic City Airport, New Jersey, 08405 USA

Artificial ice shapes of various geometric fidelity were tested on a wing model based on the Common Research Model. Low Reynolds number tests were conducted at Wichita State University's Beech Memorial Wind Tunnel, and high Reynolds number tests were conducted at ONERA's F1 wind tunnel. The aerodynamic performance data from the two facilities were compared at matched or similar Reynolds and Mach number to ensure that the results and trends observed at low Reynolds number could be applied and continued to high Reynolds number. For both clean and iced configurations, the data from Wichita State University and F1 agreed well at matched or similar Reynolds and Mach numbers. The lift and pitching moment curves agreed very well for most configurations. There appeared to be 0.2-0.3° offset in the angle of attack between the Wichita State University and F1 data, possibly due to different flow angularities in the test sections of the two facilities. There was also an offset in the drag values between the two facilities from an unknown cause. Overall, the data compared very well between the low Reynolds number test at Wichita State University tunnel and the high Reynolds number test at F1. This indicated that data from the low Reynolds number tests could be used to understand iced-swept-wing aerodynamics at high Reynolds number.

Nomenclature

b	=	Model span
c	=	Model chord
x	=	Model coordinate in chordwise direction
y	=	Model coordinate in spanwise direction
C_D	=	Drag coefficient
$C_{D,0.6}$	=	Drag coefficient at $C_L = 0.6$
$C_{D,min}$	=	Minimum drag coefficient

---

[*] Engineer V, Icing Branch, 21000 Brookpark Rd., Senior Member AIAA.
[†] Research Aerospace Engineer, Icing Branch, 21000 Brookpark Rd., Associate Fellow AIAA.
[‡] Research Associate, Dept. of Aerospace Engineering, 306 Talbot Lab, 104 S. Wright St., Member AIAA.
[§] Research Assistant Professor, William E. Boeing Department of Aeronautics and Astronautics, Guggenheim Hall Room 211, Box 352400, Member AIAA.
[**] Engineer, Aircraft Icing Research Program, ANG-E282, Bldg. 210.

C_L	=	Lift coefficient
$C_{L.max}$	=	Maximum lift coefficient
$C_{L,use}$	=	Usable lift coefficient
C_M	=	Pitching moment coefficient
C_p	=	Pressure coefficient
CRM65	=	Common Research Model 65% scale
M	=	Mach number
MAC	=	Mean aerodynamic chord
ONERA	=	Office National d'Etudes et Recherches Aérospatiales
p_0	=	Freestream total pressure
q_∞	=	Freestream dynamic pressure
Re	=	Reynolds number
RLE	=	Removable leading edge
α	=	Angle of attack
α_{stall}	=	Stall angle of attack
Λ	=	Sweep angle

I. Introduction

Understanding the aerodynamic effects of ice accretion on large, swept-wing transport class aircraft is a very complex problem. Most of the data that exist in open literature on the aerodynamic effects of icing are limited to straight (or un-swept) wing sections and usually at low Reynolds number (*Re*). Very little data exist in the literature on the aerodynamic effects of ice accretion on swept wings, especially near flight Reynolds number. In order to address this shortcoming, a collaborative research effort sponsored by NASA, the Office National d'Etudes et Recherches Aérospatiales (ONERA), and the Federal Aviation Administration (FAA) with the support of university and industry partners is currently being conducted.[1]

The main objectives of this research area are as follow:

1. Generate a database of experimental ice accretion shapes on large swept wings in order to evaluate 3D icing simulation tools.
2. Develop a systematic understanding of the aerodynamic effects of icing on swept wings including: Reynolds and Mach number effects, important flowfield physics, and fundamental differences from 2-D.
3. Determine the level of ice-shape geometric fidelity required for accurate aerodynamic simulation of swept-wing icing effects.

The baseline aircraft configuration chosen for this study was the CRM65, a 65% scale version of the Common Research Model (CRM) geometry developed for the American Institute of Aeronautics and Astronautics Drag Prediction Workshop.[2] It was representative of a Boeing 757 sized modern transport aircraft with a geometry that was available to the public. The first objective has been completed, and the results were reported by Broeren, et al.[3] In order to develop an understanding of the aerodynamic effects of icing on swept wings, geometric simulations of experimental ice accretions (obtained during the first objective listed above) were attached to swept-wing models and tested in dry-air tunnels. This followed a method that was used on a previous research program using a straight wing configuration.[4]

Past experimental studies with leading-edge ice shapes on straight wings[4,5,6,7,8] have shown that aerodynamic results obtained at low Reynolds number (~1 million) could be applied to flight Reynolds number (~10 to 20 million) without much correction to the data. This was also expected for iced swept wing configurations. Because of this, the majority of ice configurations tested in this research effort were conducted at low Reynolds numbers in the Wichita State University (WSU) atmospheric tunnel using an 8.9% scale model of the CRM65 wing, with resulting Reynolds number of 0.8 to 2.4×10^6. The economical nature of this facility allowed for numerous configurations to be tested, as well as detailed flowfield measurements to be obtained. High Reynolds number testing was also performed at the ONERA F1 tunnel using a 13.3% scale model of the same full-scale wing, with resulting Reynolds number of 1.6 to 12×10^6. This allowed results to be obtained near flight *Re*, which is around 20×10^6. The high Reynolds number tests were performed with a more limited number of ice configurations (due to much higher operational cost of the facility) and were used to verify that the results from the low Reynolds number tests were applicable to near flight Reynolds

number. Similar approach has been used in the past with varying degrees of success.[6,8] It was often quite difficult to match the aerodynamic performance of clean airfoil or wing models of different scales at matched Reynolds number. Some of the reasons were wing and airfoil geometries not being identical, different aspect ratios of 2D models, and models of different scales having different blockage effects in the test section. Iced configurations typically yielded much better results because iced shapes tend to mask some of these effects.

   During this study careful consideration was used to minimize the effects listed above in order to have a better match of the data between the low and high Reynolds number tests using models of different scale. This paper presents the aerodynamics results from ice shapes that were tested at both WSU and F1 tunnels at overlapping Reynolds and Mach numbers. If good agreement can be shown between WSU and F1 tunnel measurements, then the results from the low Reynolds number tests could be applied to high, near-flight Reynolds number with better confidence.

II.   Wind Tunnel Facilities, Models, and Experimental Methods

A.   Wind Tunnel Facilities

   The low Reynolds number tests were carried out in the Walter H. Beech Wind Tunnel at Wichita State University (WSU), in Wichita, Kansas. The high Reynolds number tests were carried out in the ONERA F1 wind tunnel located in Mauzac, France. The WSU tunnel is an atmospheric, closed-return, subsonic tunnel with a 7x10 ft. test section. The maximum speed at the test section is approximately 350 ft/s, with a corresponding Re/ft of 1.8×10^6/ft. The F1 tunnel is a pressurized, closed return tunnel with an 11.5x14.8 ft test section. It can be pressurized to 56 psi. The maximum Mach number of 0.36 (at 22 psi) and maximum Reynolds number of 6.1×10^6/ft. (at 56 psi) can be generated.

   The Reynolds and Mach number combinations are shown in Table 1 for the low Reynolds number test at WSU and in Table 2 for the high Reynolds number test at F1. Reynolds number of 1.6×10^6 was run in both WSU and F1. However, at this Reynolds number, Mach number was 0.18 in the WSU tunnel and 0.09 in the F1 tunnel. The F1 tunnel cannot operate at below atmospheric pressures and does not have the ability to operate at cryogenic temperatures, so both Re and M cannot be matched when comparing to an atmospheric tunnel running a smaller chord model, as was the case in this study. In this paper ($Re = 1.6 \times 10^6$, $M = 0.18$) condition from the WSU tunnel is primarily compared to ($Re = 1.6 \times 10^6$, $M = 0.09$) and ($Re = 2.7 \times 10^6$, $M = 0.18$) conditions from F1 tunnel and are highlighted yellow in Tables 1 and 2.

Table 1. Reynolds and Mach number conditions for WSU Tunnel.

Reynolds Number	Mach Number	q_∞ (psi)
0.8×10^6	0.09	0.08
1.6×10^6	0.18	0.30
2.4×10^6	0.27	0.69

Table 2. Reynolds and Mach number conditions for F1 Tunnel.

Reynolds Number	Mach Number				
	0.09	0.18	0.23	0.27	0.34
1.6×10^6	$p_0 = 18.9$ psi $q_\infty = 0.10$ psi				
2.7×10^6	$p_0 = 30.5$ psi $q_\infty = 0.17$ psi	$p_0 = 16.0$ psi $q_\infty = 0.35$ psi			
4.0×10^6	$p_0 = 46.4$ psi $q_\infty = 0.26$ psi	$p_0 = 23.2$ psi $q_\infty = 0.52$ psi	$p_0 = 18.9$ psi $q_\infty = 0.65$ psi	$p_0 = 16.0$ psi $q_\infty = 0.78$ psi	
6.8×10^6		$p_0 = 39.2$ psi $q_\infty = 0.88$ psi	$p_0 = 31.9$ psi $q_\infty = 1.1$ psi	$p_0 = 27.6$ psi $q_\infty = 1.3$ psi	$p_0 = 21.8$ psi $q_\infty = 1.7$ psi
9.6×10^6		$p_0 = 55.1$ psi $q_\infty = 1.2$ psi			
12.0×10^6			$p_0 = 55.1$ psi $q_\infty = 2.0$ psi		

The wind-tunnel models were installed on a turntable that provided angle of attack actuation in both facilities. The load measurements were obtained a using six-component force balance located beneath the turntable floor. In the WSU tunnel, the angle of attack sweeps were obtained utilizing a "pitch and pause" method, where the angle of attack was paused during the force measurements. In the F1 tunnel, the angle of attack was varied continuously at 0.1°/sec, and the load measurements were obtained during this continuous sweep. Additional detail concerning the WSU tunnel can be found in Woodard, et al.[9] and detail concerning the F1 tunnel can be found in Broeren, et al.[10]

B.   Wind-Tunnel Models

The wing models used in this study were geometrically scaled versions of the CRM65 semi-span wing. The F1 model was geometrically equivalent to the WSU model but scaled up by a factor of 1.5. Table 3 shows the summary of geometric parameters of these models, and Fig. 1 shows the planform with key dimensions. Other than the geometric scale, the wing geometries were identical.

Table 3. Wing model geometry parameters.

| Wing Parameter	WSU	F1
Scale	8.9%	13.3%
Span	5 ft (60 in)	7.5 ft (90 in)
MAC	1.39 ft (16.67 in)	2.08 ft (25.01 in)
Area	6.01 ft^2 (865.3 in^2)	13.55 ft^2 (1951 in^2)
Volume	0.617 ft^3 (1069 in^3)	2.09 ft^3 (3604.5 in^3)
Aspect Ratio	8.3	
Taper Ratio	0.23	
Root Chord	2.25 ft (27 in)	3.38 ft (40.5 in)
Tip Chord	0.52 ft (6.19 in)	0.77 ft (9.28 in)
Root α	4.4°	
Tip α	-3.8°	
1/4-chord Λ	35°	
Leading edge Λ	37.2°	
Location of rotation center	x = 19.37 in, z = 0	x = 29.05 in, z = 0
Location of 0.25*MAC*	x = 17.49 in, z = 0	x = 26.23 in, z = 0
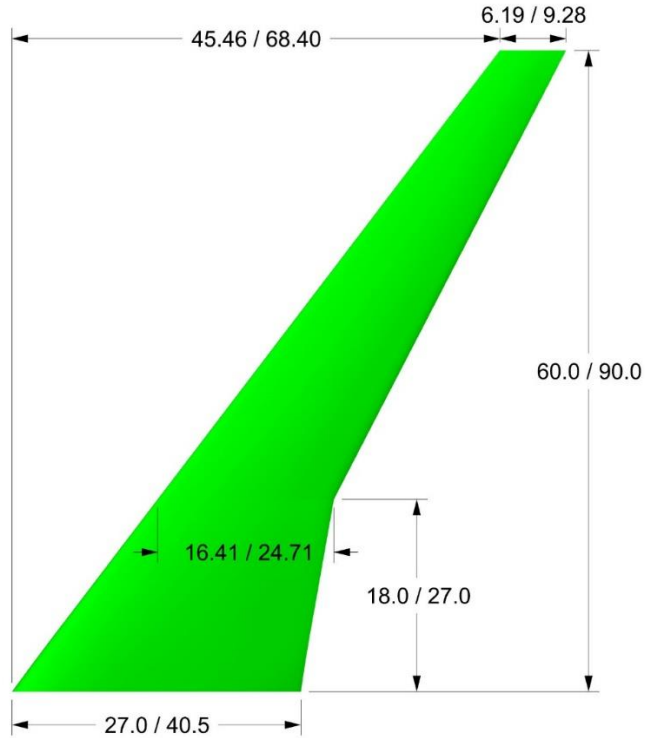
Figure 1. WSU and F1 CRM65 semi-span wing planform with key dimensions labeled in inches (WSU on left and F1 on right).

The WSU model was machined out of aluminum. It featured a removable leading edge (RLE) design that facilitated a rapid and repeatable installation of artificial ice shapes. This approach has been used very effectively in previous icing aerodynamic studies.[4,11,12] One version of the RLE consisted of clean airfoil contour and was used for testing of the clean (i.e. un-iced) wing configurations. Another version had the leading edge cut out so that artificial ice shapes could be bolted on. The F1 model also featured a RLE design. However, the main body was machined out of stainless steel because aluminum did not provide enough rigidity for high dynamic pressure testing in F1. The removable leading edge was machined from aluminum in order to reduce the weight during the ice-shape configuration changes.

The models were installed vertically on turn tables in both of the tunnels, as shown in Fig. 2. Non-metric circular splitter plates were used to place the models above the test section floor boundary layer. Both of the models were instrumented with surface pressure taps in order to obtain pressure distributions. On the WSU model, there were 219 taps distributed over 6 streamwise rows and 4 normal rows, as shown in Table 4. On the F1 model, there were 243 taps distributed over 7 streamwise rows, as shown in Table 5.
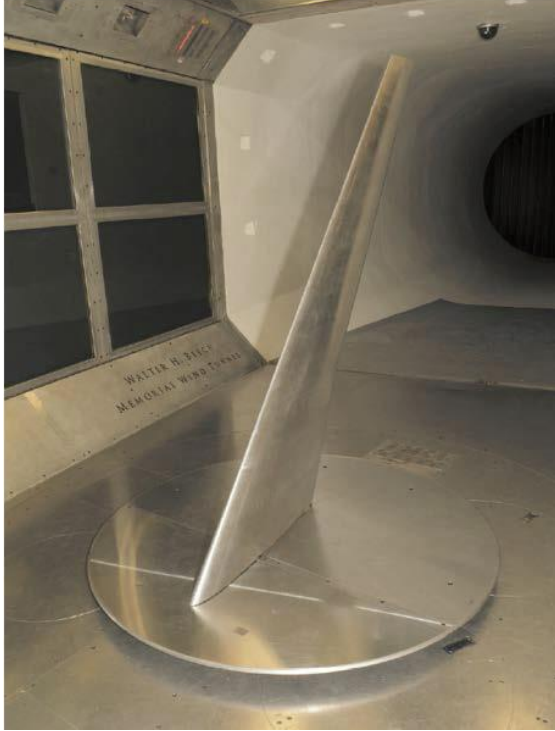
a) WSU model

b) F1 model
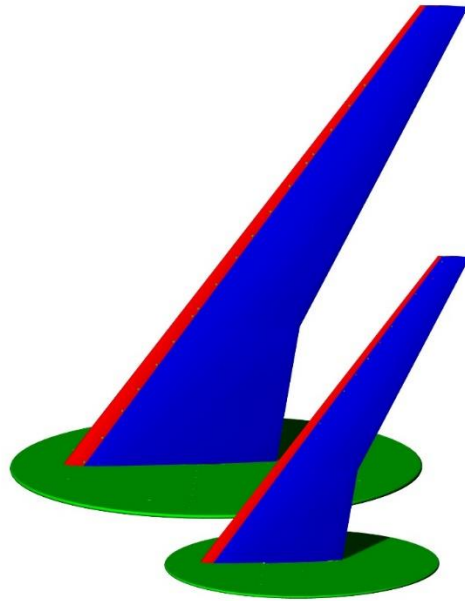
c) Models compared at same scale

Figure 2. CRM65 semi-span wing models.

Table 4. Surface pressure taps on the WSU model.

Row Identifier	Orientation	Spanwise Location (y/b)*	Taps in RLE	Upper Surface	Lower Surface	Total Taps
1	Normal	0.11	3	12	0	12
2	Streamwise	0.11	13	19	11	31
3	Streamwise	0.28	13	18	11	30
4	Normal	0.44	4	16	0	16
5	Streamwise	0.44	12	18	10	29
6	Normal	0.60	4	16	0	16
7	Streamwise	0.60	13	18	10	29
8	Normal	0.81	4	16	0	16
9	Streamwise	0.81	13	18	10	29
10	Streamwise	0.9	3	11	0	11

Table 5. Surface pressure taps on the F1 model.

Row Identifier	Orientation	Spanwise Location (y/b)	Taps in RLE	Upper Surface	Lower Surface	Total Taps
1	Streamwise	0.11	20	25	13	38
2	Streamwise	0.28	22	25	13	38
3	Streamwise	0.44	22	25	13	38
4	Streamwise	0.60	22	25	13	38
5	Streamwise	0.71	22	25	13	38
6	Streamwise	0.81	22	25	13	38
7	Streamwise	0.91	7	15	0	15

C. Aerodynamic Measurements

The primary aerodynamic measurements (C_L, C_M, and C_D) were obtained by the six-component force balance used at the two facilities. The pitching moment coefficients were calculated about the 0.25 mean aerodynamic chord (*MAC*) location. The surface pressures (C_p) were obtained by the facility pressure systems. The measurements from the WSU tunnel were obtained at paused angles of attack at every 0.25° to 1°, while the measurements from the F1 tunnel were obtained at continuous 0.1°/sec angle of attack sweep. The data were conditionally averaged into 0.5° angle of attack increments using a ±0.15° window based on the geometric (uncorrected) angle of attack. For example, data acquired over the interval $3.85° \leq \alpha \leq 4.15°$ were used to create conditionally averaged values for $\alpha = 4°$.

The WSU measurements were corrected with the standard procedure for 3-D models described in Pope, et al.[13] More detailed implementation of the corrections can be found in the WSU facility report.[14] The F1 measurements were corrected with an in-house ONERA method.[15] The F1 measurements were also corrected using the method employed at WSU to understand the implications of utilizing the different wall correction methods.

The uncertainties for the aerodynamic coefficients are shown in Tables 6 and 7. They were calculated using the "root sum square" method outlined in Coleman and Steele[16] and Kline and McClintock.[17] Detailed assumptions and analysis used to generate the uncertainties for these tests can be found in Woodard, et al.[9] (for WSU) and Torz-Dupuis[15] (for F1). It is important to note that the uncertainties for the F1 test appear large, but they are for $q_\infty = 0.35$ psi, while the maximum q_∞ tested was 2 psi. The uncertainties were lower at most of the conditions tested at F1 since they were at higher q_∞. However, for the lower q_∞, the uncertainties were higher.

Table 6. WSU tunnel aerodynamic coefficient uncertainties.
(Clean model, $Re = 1.6 \times 10^6$, $M = 0.18$, $\alpha = 5°$).

Variable	Reference Value	Absolute Uncertainty	Relative Uncertainty (%)
C_L	0.5566	0.0047	0.84
C_D	0.0220	0.0013	6.12
C_M	-0.2169	0.0020	0.92

Table 7. F1 tunnel aerodynamic coefficient uncertainties.
(Clean model, $Re = 2.7 \times 10^6$, $M = 0.18$, $\alpha = 5°$).

Variable	Reference Value	Absolute Uncertainty	Relative Uncertainty (%)
C_L	0.5749	0.0164	2.85
C_D	0.0202	0.0035	17.37
C_M	-0.2285	0.0083	3.63

D. Boundary-Layer Trips

The models were tested with boundary-layer trips applied near the leading edge on both upper and lower surfaces of the wing. The trips consisted of CADCUT trips dots which is an off-the-shelf product available in discrete sizes. On the WSU model, they were sized to trip the boundary layer at Reynolds number of 1.6×10^6. Trip height of 0.004" were used on the upper surface, and trip height of 0.0114" were used on the lower surface. For the F1 test, these heights were geometrically scaled to account for a model size that was 1.5 times larger. In this paper, comparisons are shown for the trips located at the same non-dimensional location for the WSU and F1 tests.

E. Artificial Ice Shapes

The artificial ice shapes were manufactured using stereo-lithography (SLA). The ice shape geometries used in this study were obtained from laser scans of ice shapes obtained during NASA Icing Research Tunnel tests with three CRM65 wing sections (from $y/b = 0.20$, 0.64, and 0.83) with full-scale leading edge.[3] These ice shape segments were interpolated and extrapolated over the entire span of the wing, then geometrically scaled to fit the subscale WSU and F1 models.[18] Figure 3 shows the photographs of the ice shapes obtained in the IRT (from the wing section at $y/b = 0.64$) that were tested in WSU and F1 as part of this study. Detailed descriptions of the ice shapes and the icing conditions used to generate them can be found in Broeren, et al.[3]

a) **Maximum Scallop**   b) **WB33 Appendix C**   C) **Small Gap Scallop**

d) Incomplete Scallop   **e) Streamwise/Rime**
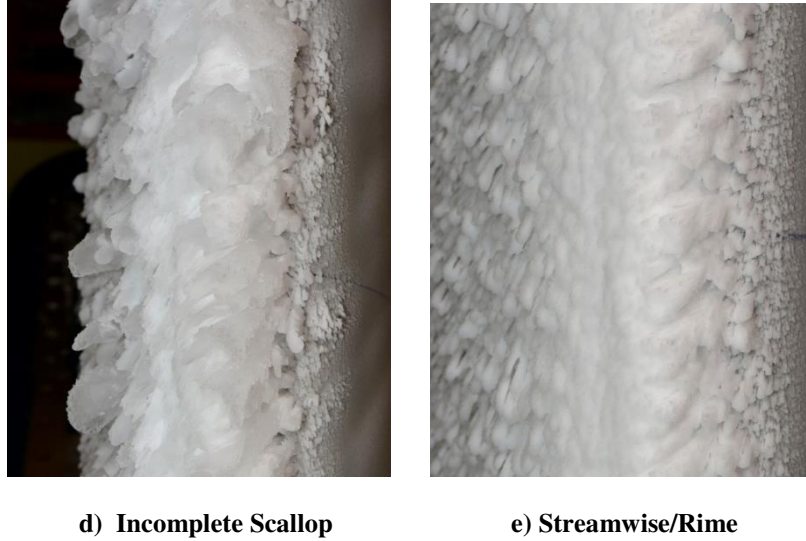
Figure 3. Photographs of IRT ice shapes used to create artificial ice shapes from *y/b* = 0.64 location on CRM65 wing.

    Artificial ice shapes of three different geometric fidelity levels were tested. The term "High Fidelity" is used to describe an artificial ice shape where an attempt was made to maintain as much of the locally 3D features from the original ice shape scan as possible.   The term "3D Smooth" is used to describe an artificial ice shape where the "3D High Fidelity" shape is smoothly lofted over the span using the largest ice shape features. An example of these two shapes is shown in Fig. 8. While the "3D Smooth" shape is three dimensional in nature over the span of the wing, locally it is essentially 2D. Another important feature is that most of the "High Fidelity" shape fits inside the "3D Smooth" shape since it is a loft of the largest features of the former shape. Finally, the "3D Smooth + Grit" is used to describe a "3D Smooth" shape with silicon-carbide grit roughness applied to the surface. For the WSU model, 60-grit was applied on double sided tape. For the F1 model, 46-grit was epoxied directly on to the ice shape. These grit size provided roughness heights that nearly matched the 3mm roughness height prescribed in the FAA Advisory Circular 25-25A[19] when geometrically scaled down to the scaled model sizes. A detailed description of how these ice shape geometries were generated can be found in Camello, et al.[18,20]
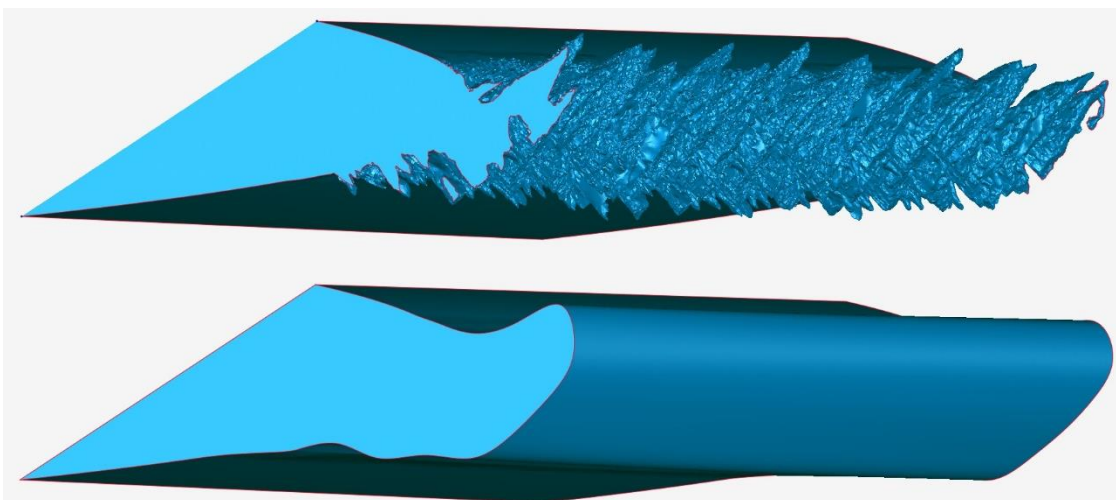
Figure 4. Comparison of "High Fidelity" artificial ice shape geometry (top) with the lower-fidelity, "3D Smooth" geometry (bottom).

III. Results and Discussions

The comparisons shown in this paper were from the clean model cases and cases where identical simulated ice shape configurations were tested in both WSU and F1 tunnels.

A. Clean and Tripped Configurations

Figure 5 shows the comparison of the two wall correction schemes that were applied to the F1 tunnel results. The plots are for the clean wing configuration at $Re = 1.6 \times 10^6$ and $M = 0.09$. The two figures on the top show the overall lift, pitching moment, and drag plots for the uncorrected data, F1 custom wall correction[15] and the correction scheme described in Barlow, Rae, and Pope.[13] The two figures on the bottom show the same plots zoomed in to regions of interest (at stall for C_L and C_M and minimum drag for C_D). The corrected lift curves were almost identical to one another, until after stall, where there are some very slight differences in the zoomed-in plot. There were more differences between the two wall correction schemes for the pitching moment and drag. However, these differences were small as well, especially when compared to the effects of different Re and M, as well as ice shape configurations, which will be shown later in this paper. Consequently, the rest of the F1 results shown in this paper are with the F1 in-house wall correction.
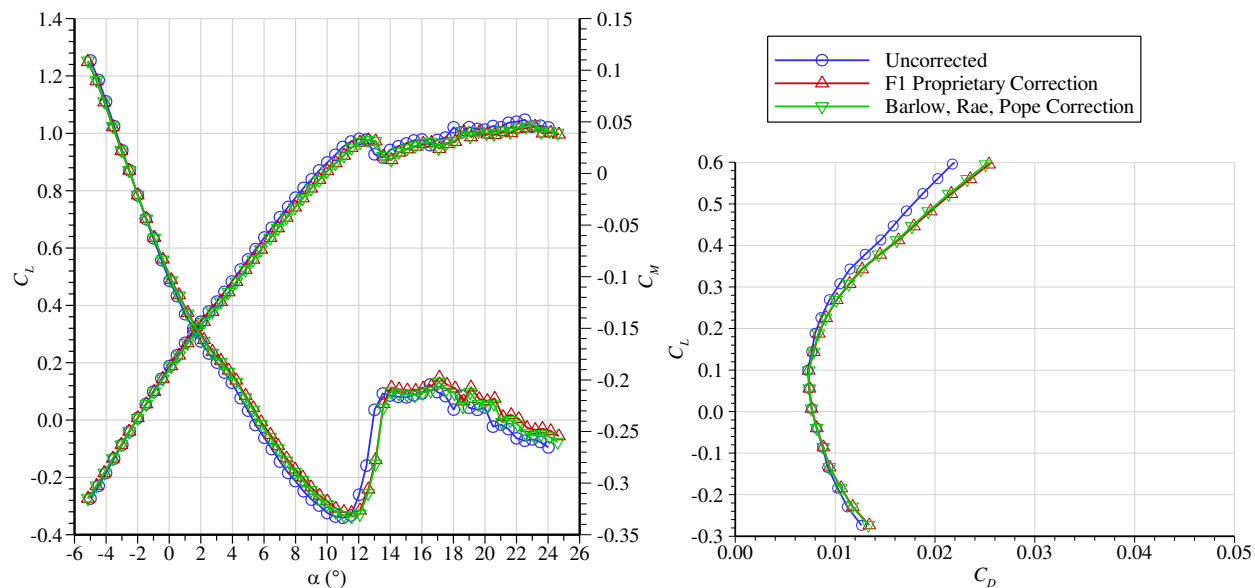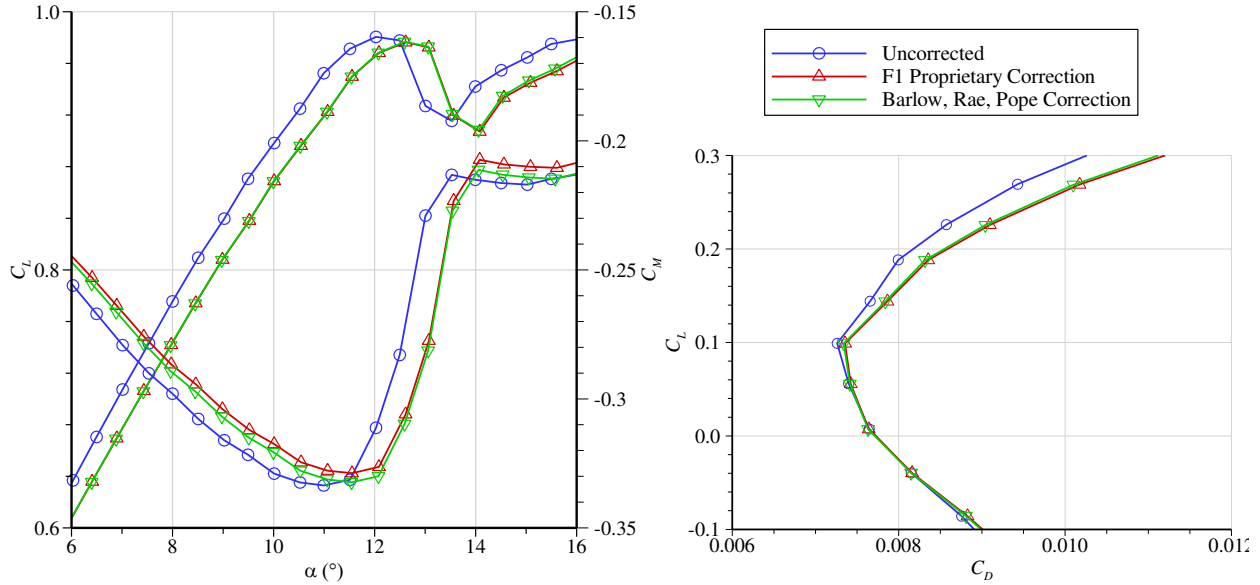
Figure 5. Wall correction schemes employed in F1. Clean wing, $Re = 1.6 \times 10^6$, M = 0.09.

One important issue to note in this comparison paper is that the angles of attack that were shown in previous papers with the WSU data[9,20,21] are incorrect. The previous WSU data contained a +0.50° angle of attack offset in the data (from what was measured with the turntable) to account for flow angularity. Subsequent analysis by the facility staff indicated that this offset was not required, and have been removed from all WSU data shown in this report. The effect of the removal of the offset is shown in Fig. 6. The figure on the left shows the overall lift and pitching moment curves for the clean wing, and the figure on the right shows the lift curve zoomed in to a region near stall. The removal of the offset shifted the lift and pitching moment curve to the left by approximately 0.5°. It did not affect the lift or pitching moment values in any other way. Consequently, removing the angle of attack offset resulted in much closer match of the WSU lift curve to the F1 lift curve at matched Re. When comparing the data in the current[10,22,23] and future reports to the previously published reports, it is important to note the change in the angle of attack.
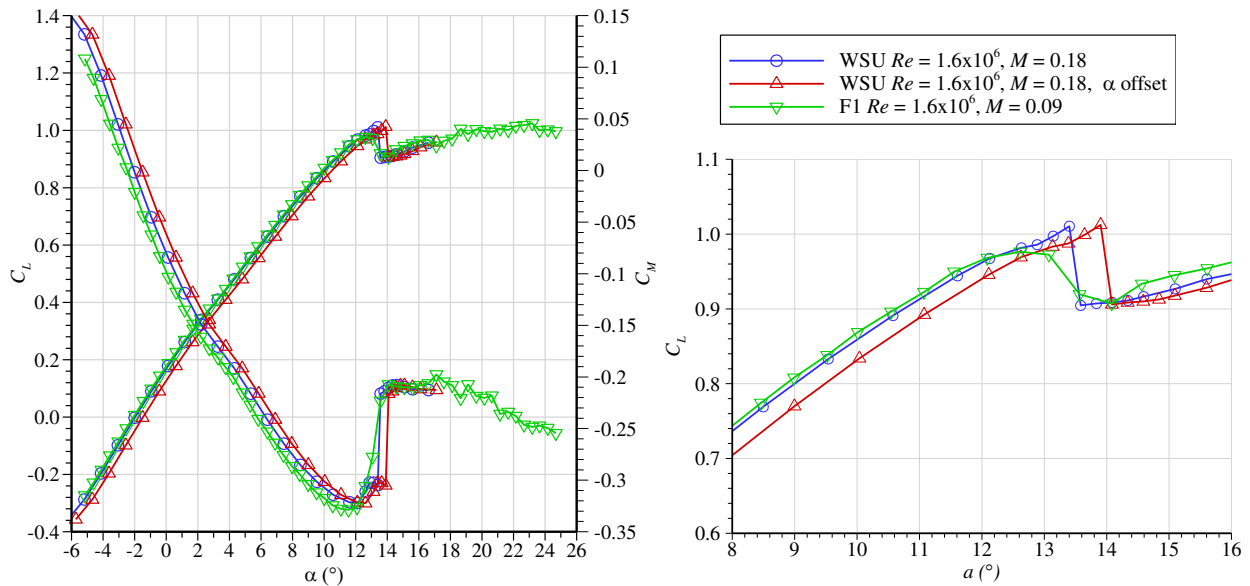
Figure 6. Angle of attack offset in previously published WSU data. Clean wing.

Figure 7 shows the clean model lift, pitching moment, and drag curves for the WSU and F1 models at matched Re and M. As stated in the introduction, it was not possible to match both Re and M for WSU and F1 facilities. Comparisons are thus shown at matched Re with M kept as close as possible and at matched M while keeping Re as close as possible. The top two figures show the overall lift, pitching moment, and drag curves. The bottom two figures show the same curves zoomed into regions of interest in order to show the differences better. Generally, the data from WSU and F1 agreed well. The F1 data at the higher Mach number had higher lift curve slope as expected from the Prandtl-Glauert effect.[24] The maximum lift coefficient for the WSU case was 1.01, which fell in between the two F1 cases ($C_{L,max} = 0.98$ for $Re = 1.6x10^6$ and $C_{L,max} = 1.04$ for $Re = 2.7x10^6$). The two F1 cases showed slightly more gradual stall than the WSU case, but this was likely due to the data averaging (over 0.30° angle of attack) that was done to reduce the noise in the F1 balance data. The stall angle of attack for the WSU case was 13.4°, while for F1 it was 12.6° for $Re = 1.6x10^6$ and 13.1° for Re=2.7x10^6. The lift values after stall agreed well between all three cases. The WSU and F1 lift curves should match exactly at the matched Mach number prior to stall, and there was an offset of approximately 0.3° in the angle of attack between the two, even after the removal of the 0.5° offset from the WSU data. This indicated that there may be differences in the test section flow angularities in the WSU and F1 tunnels. The pitching moment curves generally showed good agreement between WSU and F1, with the break in the C_M curve (associated with stalling wing) occurring at similar angles of attack. The drag curves show some discrepancies between WSU and F1 data. The F1 drag at $Re = 1.6x10^6$ and $M = 0.09$ is higher than at $Re = 2.7x10^6$ and $M = 0.18$ as expected (due to Re effects). However, the WSU drag was higher than the F1 drag even at matched Re. The reason for this mismatch was not clear but could have been due to the measurement uncertainties in the F1 data (operating at the very low end of the q_∞ range).
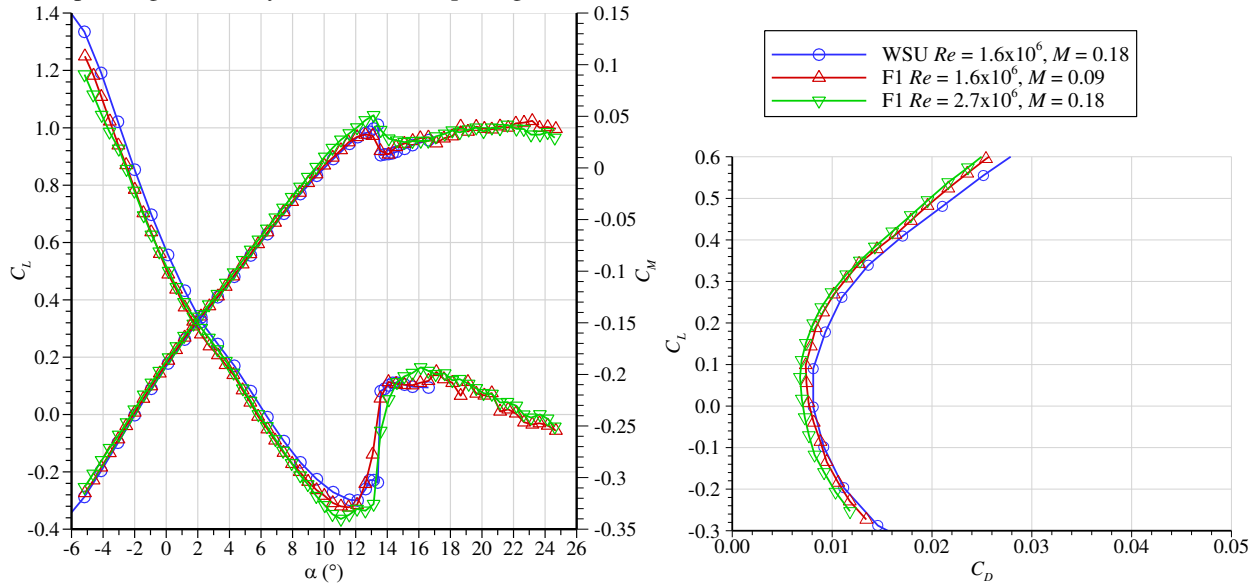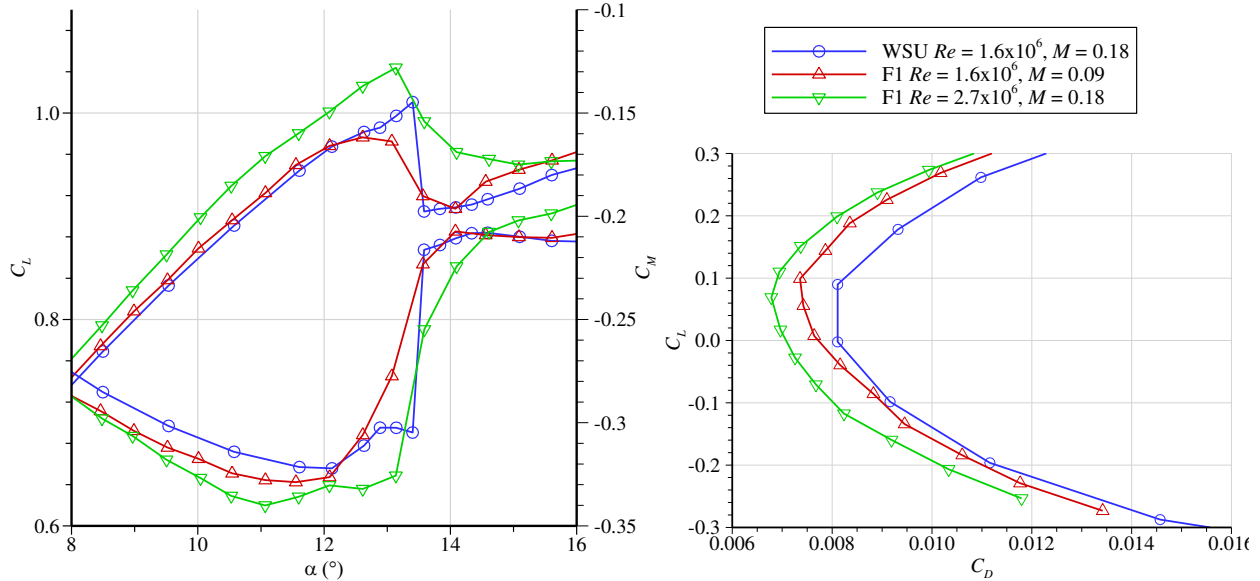
Figure 7. Clean wing performance comparison.

Figure 8 shows the comparison of surface pressure coefficients between the WSU and F1 tests. The pressures were from the spanwise taps at $y/b = 0.60$. This corresponded to pressure tap row 7 on the WSU model (Table 4) and pressure tap row 4 on the F1 model (Table 5). Figure 8a shows the surface pressures at $\alpha = 6°$, and Fig. 8b shows the surface pressures at $\alpha = 10°$ (both at uncorrected angles of attack). At $\alpha = 6°$, the wing was still in the linear portion of the lift curve and the flow remained completely attached over the entire span. At $\alpha = 10°$, the wing was nearing stall, which occurred around 13°. Figure 8a shows that at $\alpha = 6°$, the surface pressures were nearly identical for WSU and F1 cases. At $\alpha = 10°$, there were some differences that were present. The WSU and F1 cases at $M = 0.18$ were nearly identical, but the F1 case at $M = 0.09$ exhibited lower pressure coefficient between the leading edge and 16% chord on the upper surface. This indicated that the flow in this region was separated for F1 case at $M = 0.09$, while on the other two cases, the flow remained attached. This is indicated in the close-up lift plots shown in Fig. 7, where the F1 case at $M = 0.09$ had slightly lower stall angle of attack when compared to the other two cases.
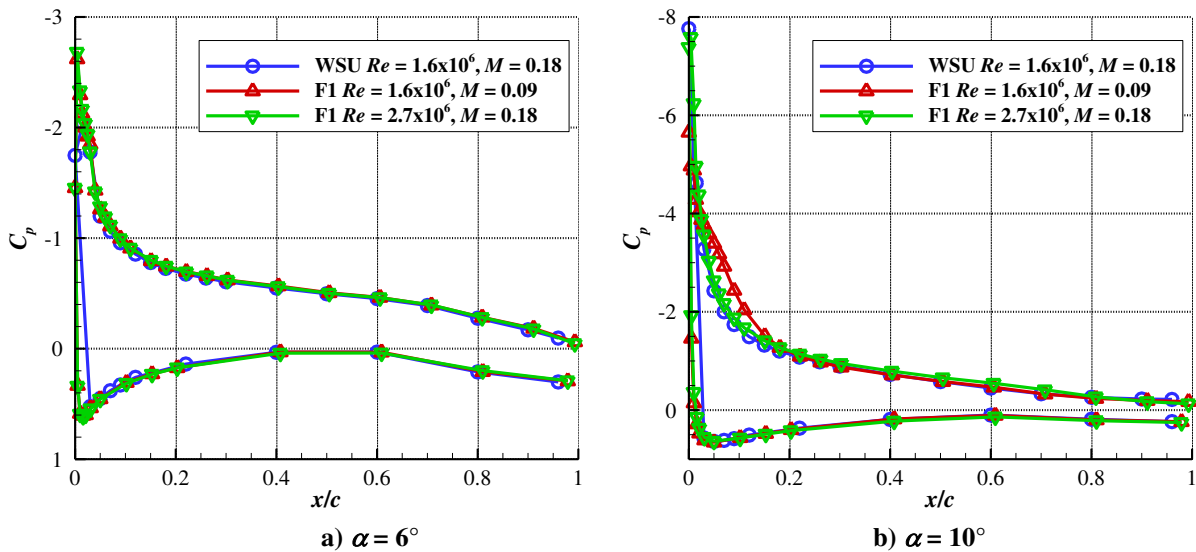

a) $\alpha = 6°$ **b) $\alpha = 10°$**

Figure 8. Clean wing surface pressure comparison ($y/b = 0.60$).

Figure 9 shows the comparison of the boundary-layer tripped wing between the WSU and F1 tests. Again the figures on the top show the overall performance curves, and the figures on the bottom show the same curves zoomed

American Institute of Aeronautics and Astronautics

in to regions of interest. The comparisons between the WSU and F1 data were generally similar to what was observed with the clean wing shown in Fig. 7. For the tripped case, the $C_{l,max}$ and α_{stall} for the WSU case were very similar to the F1 case at $Re = 1.6 \times 10^6$ and $M = 0.09$. The F1 data showed slighted sharper stall than the WSU data. The differences in $C_{l,max}$ and α_{stall} values for the F1 case at $Re = 2.7 \times 10^6$ appeared to be more substantial. However, this may have been due to an anomalous data point at $\alpha = 13.7°$. If that point is not considered, the $C_{l,max}$ and α_{stall} values becomes much closer to the other two cases. The pitching moment curves compared very well between the WSU and F1 data. The drag data followed the same trends observed in the clean wing comparison where the WSU drag was higher than the F1 drag at matched Re.
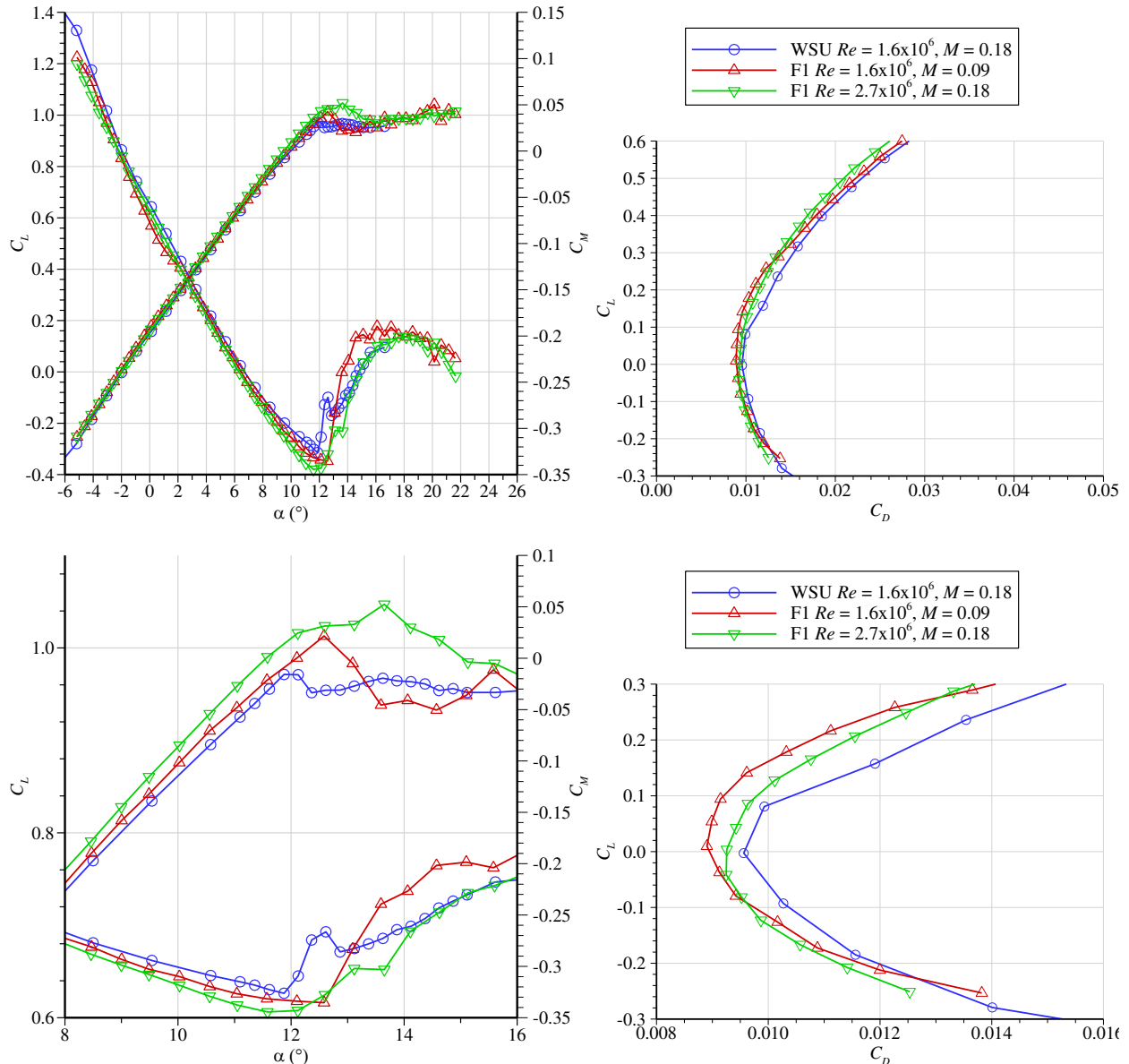
Figure 9. Tripped wing performance comparisons

B. Iced Configurations

Figure 10 shows the comparison of the aerodynamic performance measurements between the WSU and F1 tests with the "Maximum Scallop High Fidelity" ice shape attached to the leading edge of the wing. The lift and pitching moment curves agreed very well at both matched Reynolds number and matched Mach number, even when the plots

American Institute of Aeronautics and Astronautics

were zoomed in to regions of interest. It is important to note that in the WSU test, the angle of attack was taken up to only 16° because by then, the flow over 90% of the span had separated and the additional lift was being generated by the inboard 10% of the span that had remained attached. This can be seen in the break in the pitching moment that started near $\alpha = 6°$, indicating onset of flow separation. However in the F1 test, the angle of attack range was increased to capture $C_{l,max}$ as traditionally defined. The break in the pitching moment curves occurred at same angle of attack for all three cases. The drag data showed that the WSU drag coefficients were higher than the F1 drag coefficients, similar to what was seen with the clean wing. The F1 data showed that there were very little Re and M effects with the Max Scallop High Fidelity ice shape, and the WSU data agreed very well (for lift and pitching moment) with F1 data even though Re and M were not both exactly matched. One item to note from the close-up lift plot is that there appears to be about a 0.3° offset between the WSU and F1 data, similar to what was seen with the clean wing data at matched Mach number.
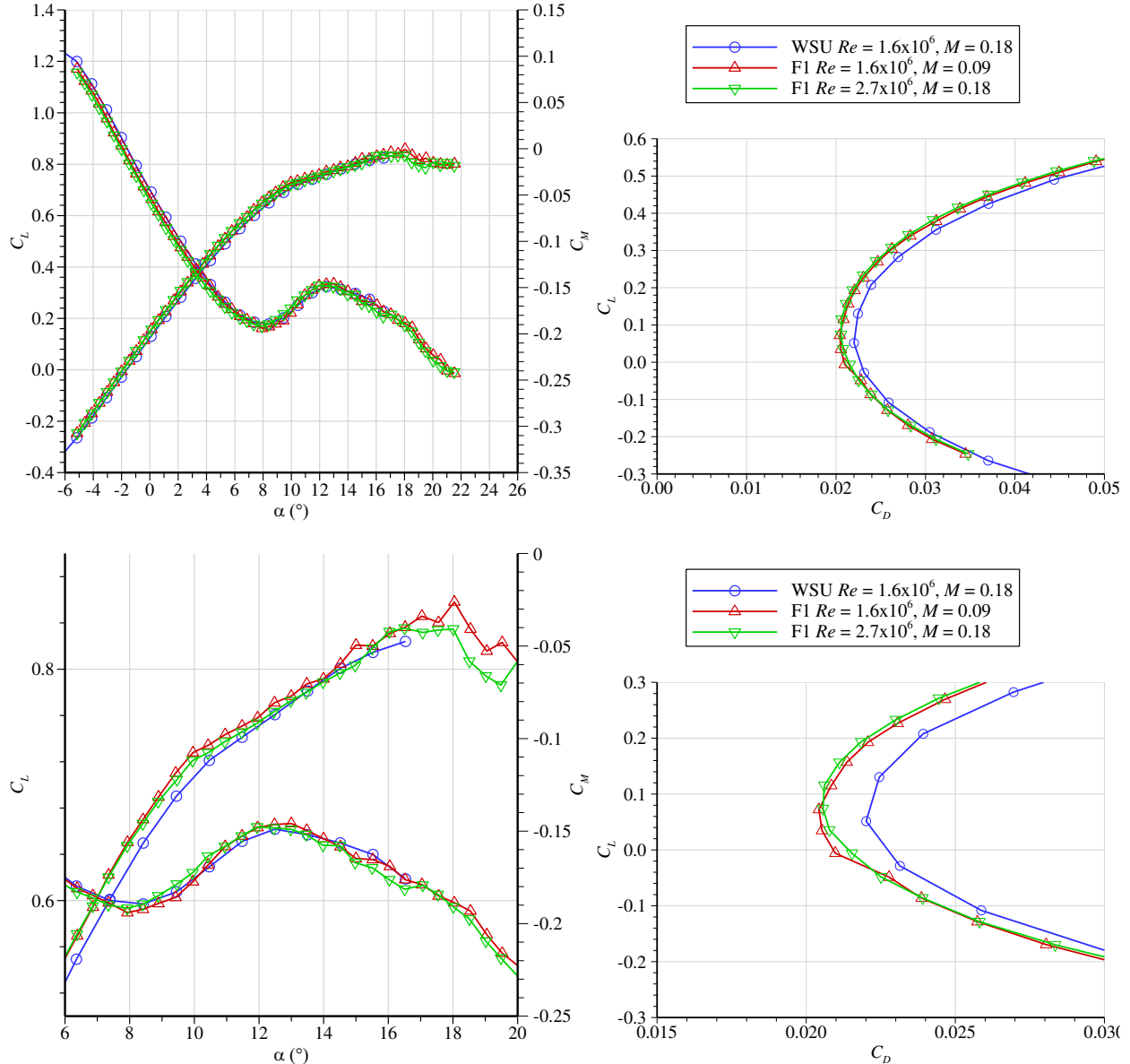
Figure 10. Max Scallop High Fidelity ice shape performance comparison.

Figure 11 shows the comparison of the surface pressures between the WSU and F1 tests with the Max Scallop High Fidelity Ice shapes at $\alpha = 6°$ and $10°$ (uncorrected angles of attack). Again, they were both from the pressure taps at $y/b = 0.60$. Pressure data are missing from the leading edge because there were no pressure taps present on the ice shapes. The fluorescent oil flow visualization and mini-tuft image from the WSU test[22] indicated that at $\alpha = 6°$

(or 6.35° corrected) the boundary layer was separated from the ice shape to $x/c = 20$ at $y/b = 0.60$. This is seen by the low pressure region due to leading edge separation that extends from the leading edge to $x/c = 0.20$. Nearly identical pressure distributions were observed for the two F1 cases at this angle of attack. At $\alpha = 10°$ (or 10.47° corrected) the flow was completely separated. This is shown by the nearly constant upper surface pressure at this angle of attack. Again, the WSU and F1 data agreed very well.

a) $\alpha = 6°$ **b)** $\alpha = 10°$
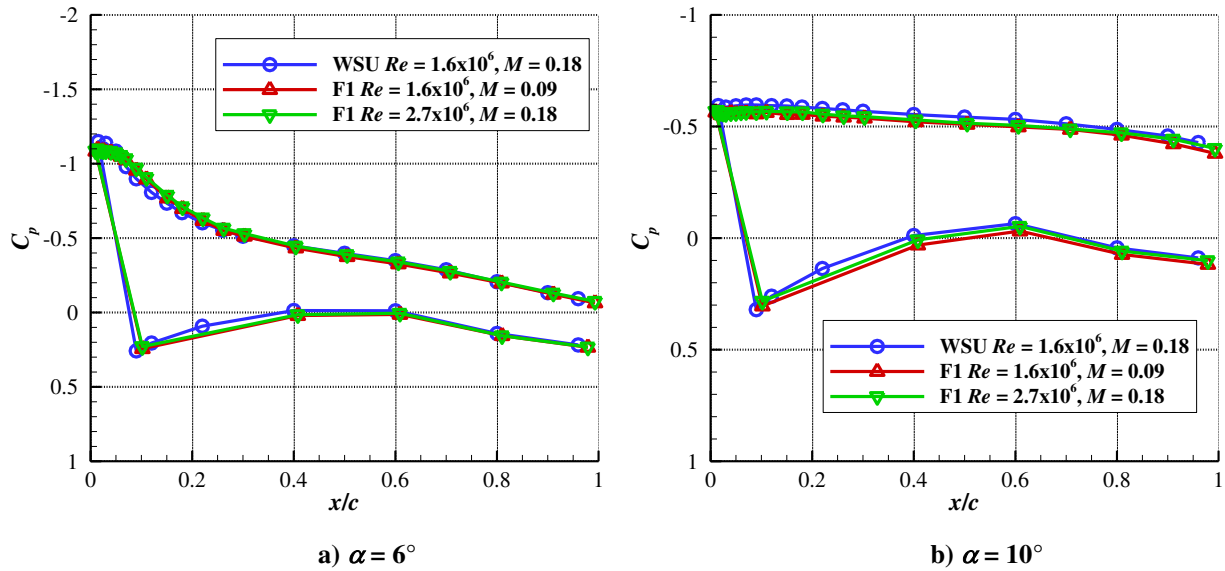
Figure 11. Max Scallop High Fidelity ice shape surface pressure comparison.

The comparison of the Max Scallop 3D Smooth ice shape is shown in Fig. 12. The figure on the left shows the overall lift and pitching moment curves and the figure on the right shows the lift curve zoomed in to the region of interest near stall. The drag data are no longer shown since the trends were nearly identical for all subsequent iced configurations and do not add much to the discussion. As with the Max Scallop High Fidelity shape, the WSU data were only taken to $\alpha = 16°$ because the flow was considered nearly completely separated by this angle of attack. The WSU data generally agreed very well with the F1 data except for an angle of attack shift of approximately 0.2°, similar to what was observed with the Max Scallop High Fidelity ice shape.
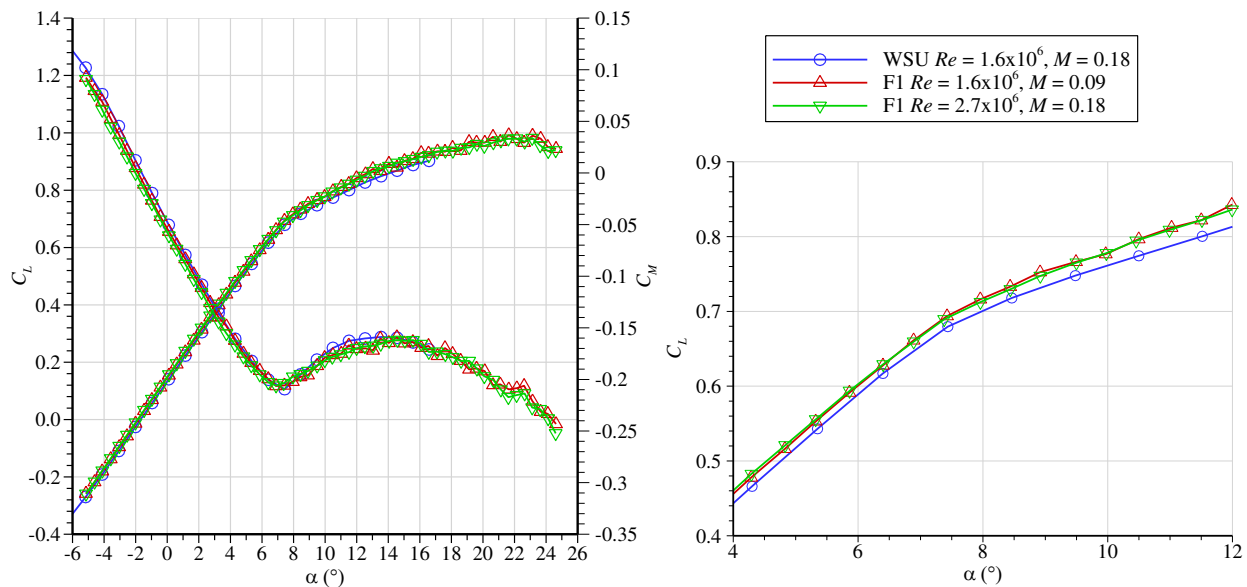

Figure 12. Max Scallop 3D Smooth performance comparisons.

Figure 13 shows the comparison of the Max Scallop 3D Smooth ice shape with the grit applied. The comparisons between the facilities look very similar to the other fidelities of the Max Scallop ice shape, where the WSU data compared very well with the F1 data except for the angle of attack offset.
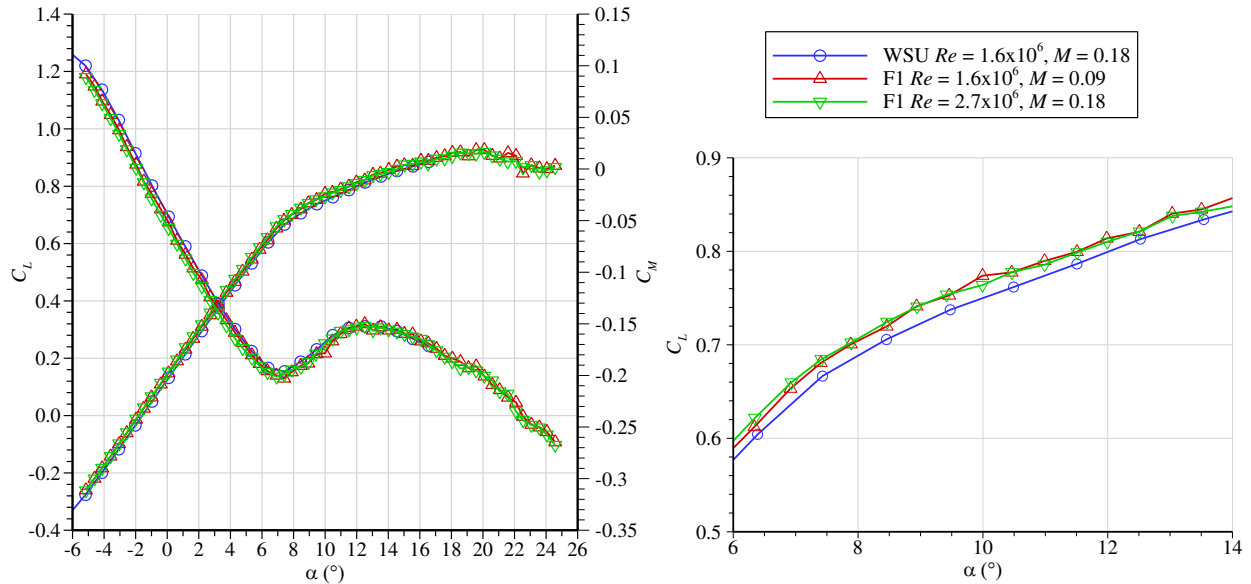

Figure 13. Max Scallop 3D Smooth + Grit ice shape performance comparisons.

Figure 14 shows the comparison of the WB33 Appendix C High Fidelity ice shape. The WSU data compared very well with the F1 data except for the angle of attack offset. Good comparisons were also observed for the Small Gap Scallop High Fidelity ice shape, as shown in Fig. 15. The comparison for the Incomplete Scallop High Fidelity ice shape is shown in Fig. 16. The WSU and F1 data did not agree was well as the other ice shapes shown previously. The WSU data had higher $C_{l,max}$ as well as α_{stall}, when compared to the F1 data. The WSU lift and pitching moment curves diverged from the two F1 cases at $\alpha = 10°$. The cause of this discrepancy was not determined, but after the F1 wind tunnel run, the clay-wax sealant that filled the gap between the SLA artificial ice shape and the aluminum leading edge part of the model was observed to have blown off over a large portion of the model span. This likely occurred during the runs at higher q_∞ and likely affects most or all of the runs for this iced configurations (since the runs with the highest pressures were performed first). This was thought to potentially have caused an air leak to form through the interface between the artificial ice shape and the model. An effort to minimize the potential of this occurring was done by taping the seam between the ice shape and the model on the lower surface. This configuration will be repeated in an upcoming test campaign at F1 in order to determine the exact cause of this discrepancy.
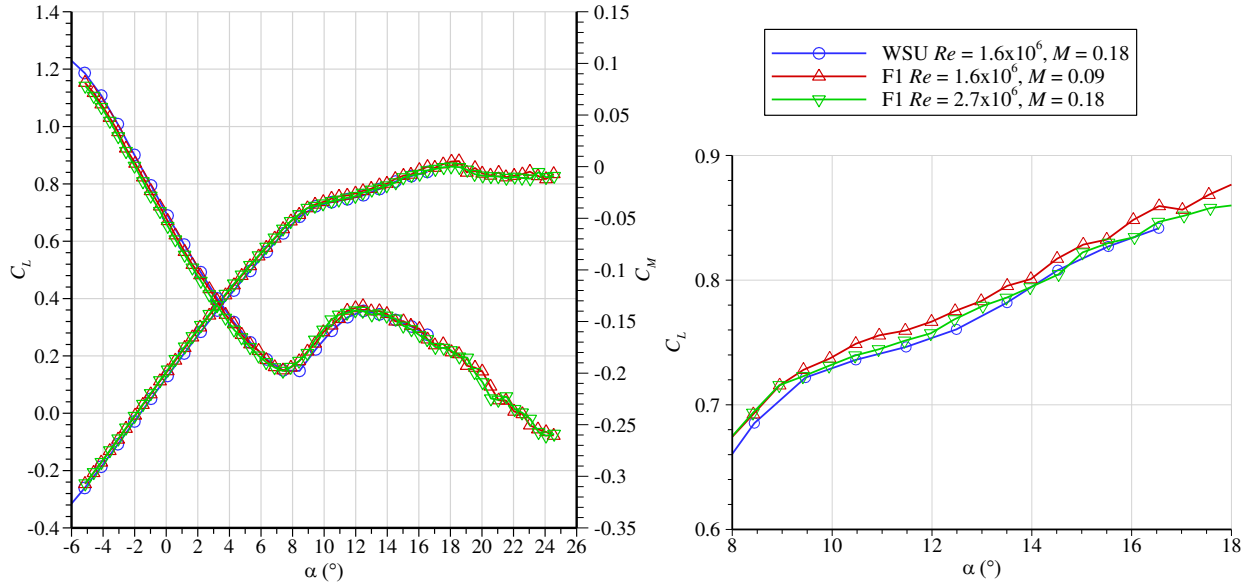
American Institute of Aeronautics and Astronautics

Figure 14. WB33 Appendix C High Fidelity ice shape performance comparison.
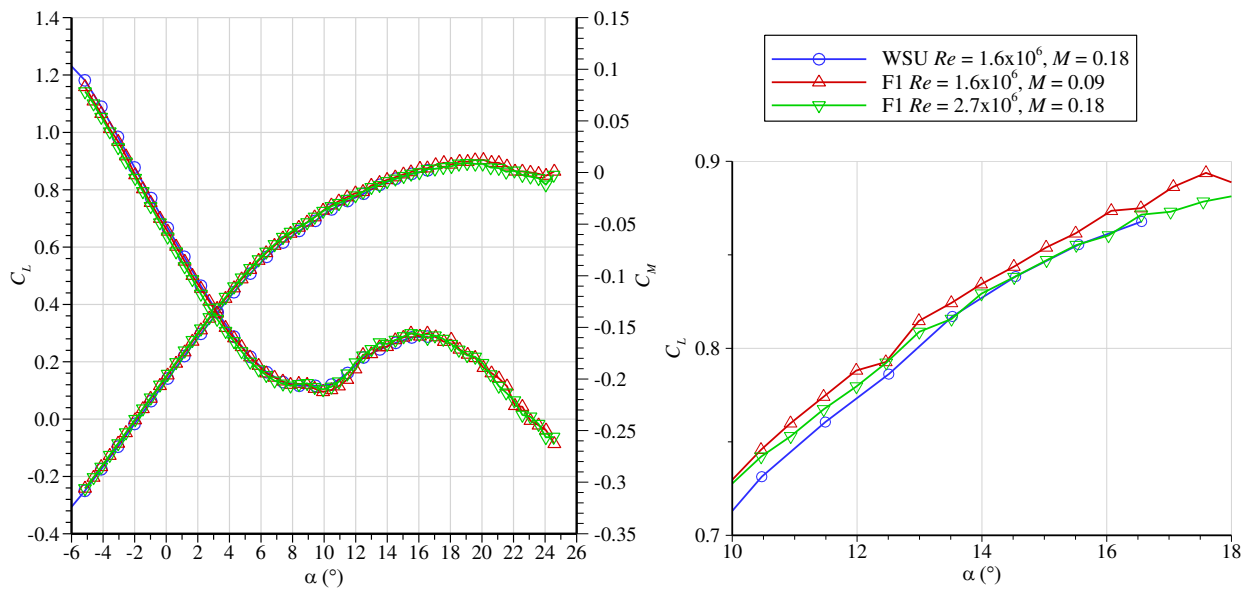
Figure 15. Small Gap Scallop High Fidelity ice shape performance comparisons.

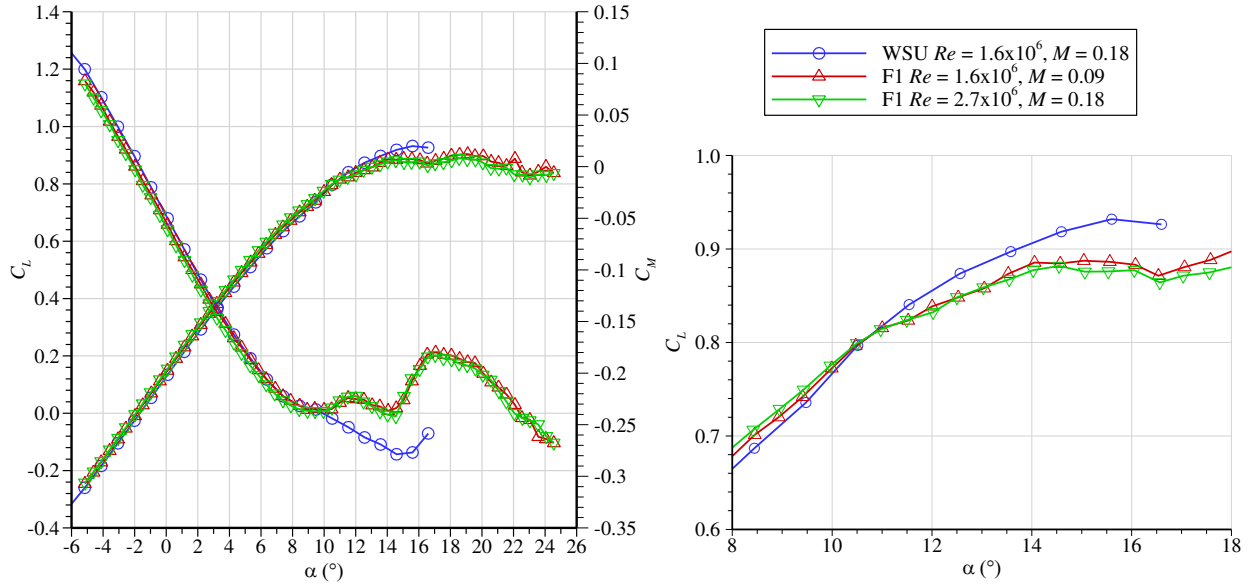American Institute of Aeronautics and Astronautics

Figure 16. Incomplete Scallop High Fidelity ice shape performance comparisons.

Figure 17 shows the Streamwise High Fidelity ice shapes tested at the WSU and F1 tunnels. The WSU and F1 comparison appeared similar to that of the Incomplete Scallop High Fidelity shape shown in Figure 16. With the angle of attack offset between the WSU and F1 data accounted for, the lift curve from the WSU data diverges from the F1 data at α of approximately 11°, as shown in the close-up lift data. This coincided with where the pitching moment curve from the WSU data diverged significantly from the F1 data. A significant removal of clay-wax sealant was not observed during the F1 test run like in the Incomplete Scallop High Fidelity case. The reason for this discrepancy is not known at this time and repeat tests with this configuration may be warranted.
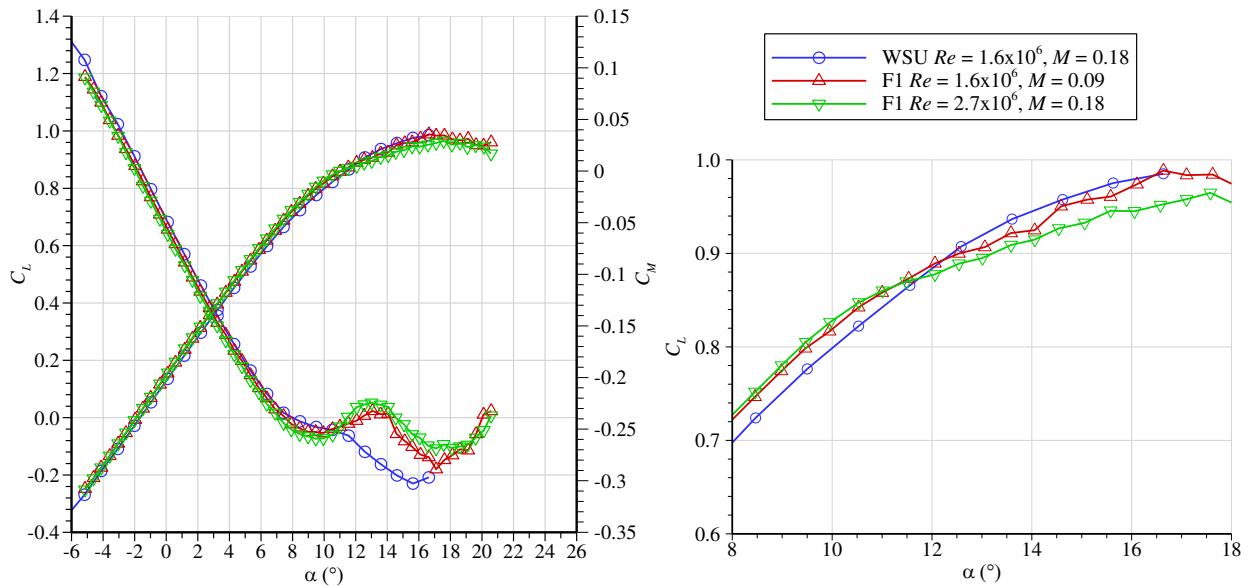

Figure 17. Streamwise High Fidelity ice shape performance comparisons.

Figure 18 shows the WSU and F1 comparisons with the Streamwise 3D Smooth ice shape. This was the most conformal of the ice shapes tested and had the largest amount of *Re* and *M* effects in both the low *Re* test at WSU[20] and the high *Re* test at F1.[10] This is shown in the F1 lift curves where $C_{l,max}$ (1.03) and α_{stall} (14.1) at $Re = 2.7 \times 10^6$

were higher than at $Re = 1.6\text{x}10^6$ ($C_{l,max} = 0.97$ and $\alpha_{stall} = 13.1°$). The lift curve slope for the $M = 0.18$ case was also slightly higher than for the $M = 0.09$ case as indicated by the lift curve being slightly higher at higher angles of attack. The $C_{l,max}$ for the WSU data was 0.98, and α_{stall} was 13.6°. The α_{stall} values at matched $Re = 1.6\text{x}10^6$ would have been even closer had the α offset between WSU and F1 data (present in all of the plots shown in this paper) been accounted for.
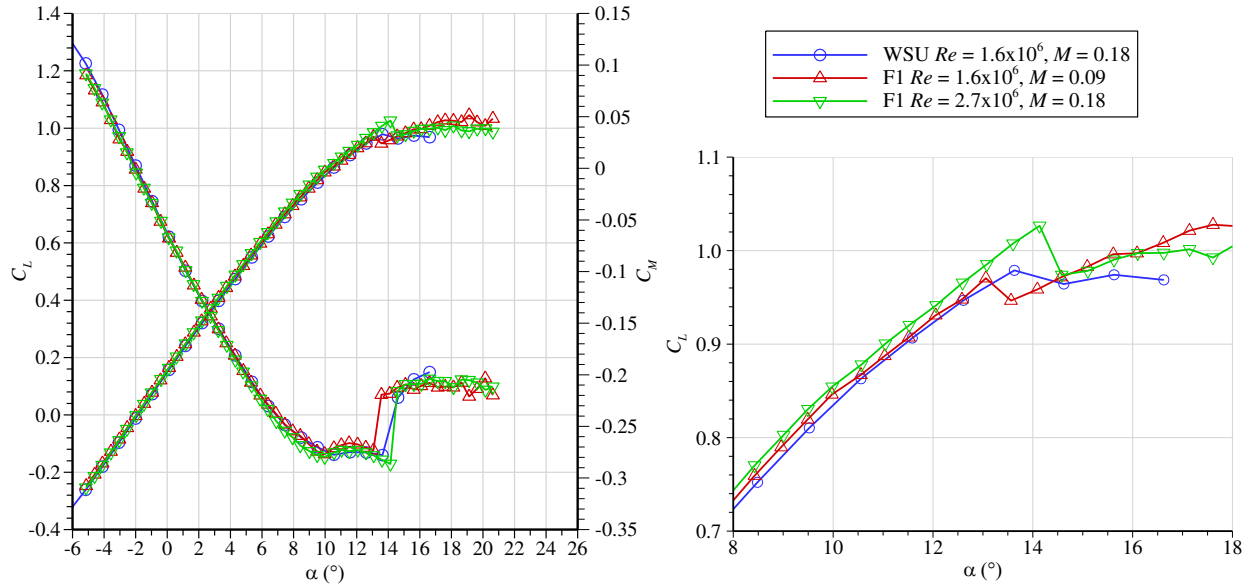

Figure 18. Streamwise 3D Smooth ice shape performance comparisons.

Figure 19 shows the comparison of the Streamwise 3D Smooth ice shape with the roughness grit. The application of the roughness eliminated much of the Re and M effects in the F1 data that were observed in the configuration without the grit (Fig. 18). The WSU lift and pitching moment curves diverged significantly from the F1 data around $\alpha = 11°$. In fact, the repeat runs at WSU showed significant differences in the lift and moment curves at around $\alpha = 11°$. As stated in Section II.E, during the WSU test, the roughness grit was applied on top of double-sided tape which was applied to the ice shapes. The repeat runs were performed using different applications of the grit, so there may have been enough variation in the application of the grit to induce a difference in the wing aerodynamic performance. Repeat grit applications were tested with the Max Scallop 3D Smooth shape at WSU with good agreement in the data. This indicated that the flow separation characteristics with the Streamwise 3D Smooth shape were more sensitive to the grit application than other shapes that were tested. This Streamwise 3D Smooth + Grit configuration will be retested in a future WSU test with the grit applied directly to the ice shape using epoxy (like in the F1 test) in order to obtain a more consistent result.
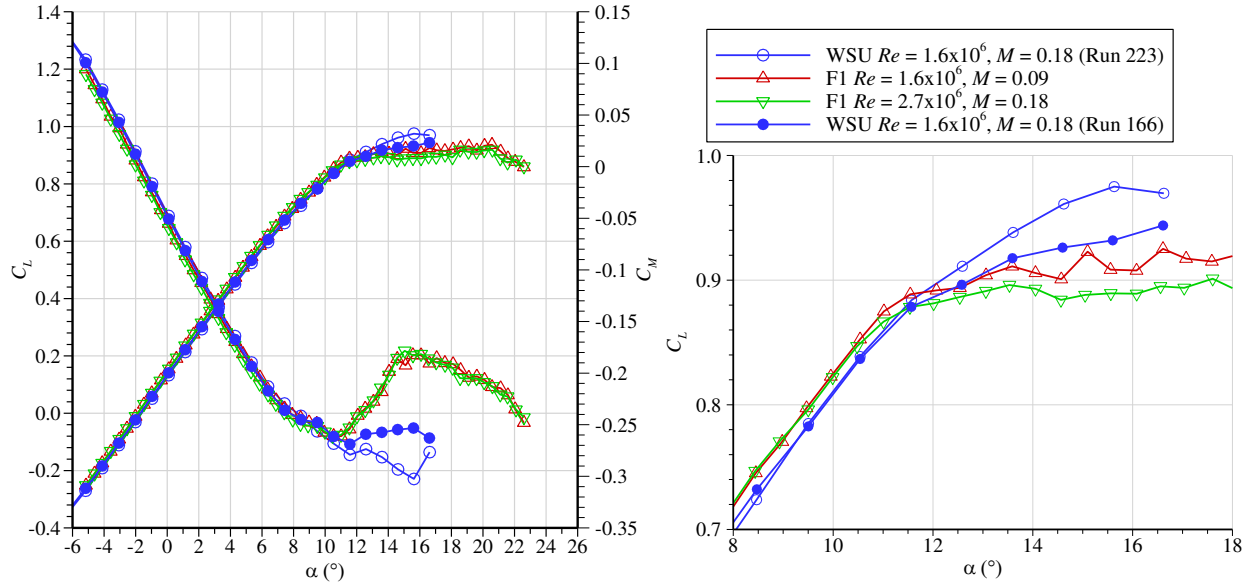
Figure 19. Streamwise 3D Smooth + Grit performance comparisons.

C. Performance Parameter Comparisons

Broeren, et al.[10] presented several performance parameters to quantify the effects of ice shape geometry on swept wing performance. Maximum lift coefficient, $C_{L,max}$, has traditionally been used as the most important and easily identifiable performance parameter. Stall angle of attack, α_{stall}, is traditionally defined as the angle of attack at which the $C_{L,max}$ occurs. For the clean wing tested in F1 at $Re = 1.6\times10^6$ and $M = 0.09$ (Fig. 7), the $C_{L,max} = 0.98$ with $\alpha_{stall} = 12.6°$. For Maximum Scallop High Fidelity ice shape tested in F1 at $Re = 1.6\times10^6$ and $M = 0.09$ (Fig. 10), $C_{L,max} = 0.86$ with $\alpha_{stall} = 18.0°$. The results from the F1 test showed that the stall angles for iced configurations were typically higher than for the clean wing, which was quite different from what was observed in prior research on straight wings or airfoils with large leading edge ice shapes where iced wings stalled at lower angles of attack. Figure 10 shows that for the Maximum Scallop High Fidelity ice shape configuration, the wing stall process began at a much lower angle of attack ($\alpha = 8°$), when compared to the clean wing, as indicated by an abrupt reduction in the lift curve slope and a large change in the slope of the pitching moment. Flow visualization from the mini-tuft images showed that the flow had started to separate at the wing tip at this angle of attack and the separation progressed towards the root with increasing angle of attack. The flow was separated over most of the wing well before the traditionally defined $C_{L,max}$ and α_{stall} was reached, with potentially large undesirable controllability issues. Because of this, the use of maximum lift coefficient and stalling angle may not necessarily be the best indicator of the stall progression on the swept, CRM65 wing with artificial ice shapes. This led to the identification of an additional performance metric that was associated with the change in the pitching-moment coefficient based on the work in 1957 by Furlong and McHugh.[25]

Furlong and McHugh identified a performance-based parameter called "usable" lift based on their review of previous work on low Re swept wings. For convenience, the authors assumed that the quarter-chord MAC location was coincident with the airplane center of gravity. Therefore, the longitudinal stability could be referred to as either stable or unstable depending on the slope of the pitching-moment curve with respect to angle of attack. The change from a negative slope to a positive slope occurs at the first local minimum in the C_M vs α curve, and stall control would be required beyond this angle of attack. The lift coefficient at this angle of attack was described as the usable lift coefficient, or $C_{L,use}$. This interpretation of usable lift implies that a certain amount of flow separation on the wing has crossed some threshold such that this value of the usable lift coefficient may be more significant than the absolute value of the maximum lift coefficient. This interpretation of usable lift is applicable to the iced-wing aerodynamic effects observed within the present data set.

Two drag-based performance parameters were also presented by Broeren, et al.,[10] based on report by Lynch and Khodadoust.[26] The first was the minimum drag coefficient ($C_{D,min}$) which was the change in the profile drag since the induced drag would be nearly zero at these angles of attack. The other parameter was based on drag at flight speed 30% above 1-g stall speed for the clean configuration. For the CRM65 wing used in this study, this was represented

by drag at $C_L = 0.6$ or $C_{D,0.6}$. A more detail description of these performance parameters can be found in Broeren, et al.[10]

The comparison of the performance parameters between the WSU and F1 data for the clean wing is shown in Fig. 20. Figure 20a shows the comparison of the maximum lift coefficient vs. Reynolds number. The F1 data shows $C_{L,max}$ at fixed Mach numbers of 0.09, 0.18, and 0.23. The WSU curve is not at fixed Mach number since the Reynolds number cannot be independently varied from the Mach number since it is an atmospheric wind tunnel. Also, in the WSU test, the $C_{L,max}$ value was not obtained for $Re = 0.8 \times 10^6$ because a classically defined $C_{L,max}$ did not occur before the angle of attack sweep was stopped at $\alpha = 16°$. Is was clearly evident from the F1 data that the clean wing exhibited both Reynolds number and Mach number effects. The $C_{L,max}$ increased with increasing Reynolds number, while it decreased with increasing Mach number. Observing this effect is only possible in wind tunnel facilities such as F1 where Re and M can be independently varied. These trends are impossible to identify in the WSU data where an increase in Re also resulted in the increase in M. However, the $C_{L,max}$ value from the WSU data at $Re = 1.6 \times 10^6$ and $M = 0.18$ compared reasonably well to F1 value at $Re = 1.6 \times 10^6$ and $M = 0.09$. Also, the $C_{L,max}$ value from WSU at $Re = 2.4 \times 10^6$ and $M = 0.27$ was close to the F1 value at $Re = 2.7 \times 10^6$ and $M = 0.23$, indicating good agreement in $C_{L,max}$ values when the Reynolds number was matched (or nearly matched) and the Mach numbers were reasonably close. Figure 20b shows the comparison of the useable lift coefficient, $C_{L,use}$, as defined by Furlong and McHugh.[25] The F1 data shows clear Reynolds number effects in the usable lift values, just like with the maximum lift. However, there was no Mach number effect between $M = 0.09$ and 0.18. The WSU data agreed well with the F1 data at $Re = 1.6 \times 10^6$ and near $Re = 2.4 \times 10^6$.

Figure 20c shows the comparison of the minimum drag values. The F1 data shows that there was no Mach number effect on the $C_{D,min}$ value. The minimum drag values decreased with increasing Reynolds number from 1.6×10^6 to 4×10^6 and then started to increase with increasing Reynolds number. The WSU data followed the trends observed in the F1 data, except for the offset of approximately 0.001 (or 10 drag counts) that was shown in Fig. 7. Figure 20d shows the comparison of the drag coefficient at $C_L = 0.6$ (or $C_{D,0.6}$). The $C_{D,0.6}$ values also exhibited no Mach number effect. However, the Reynolds number effects were slightly different in that the $C_{D,0.6}$ values decreased with increasing Reynolds number in all Re range. The WSU data followed the trends shown in the F1 data, although with an offset of approximately 0.002 (or 20 drag counts).

The performance parameters from the clean wing showed that for lift values, a pressurized tunnel is required to study the independent effects of Re and M on clean wing. However, the WSU data did match the F1 data at matched Reynolds number and when Mach numbers were reasonably close. For drag values, a pressurized tunnel was not required since there was no M effect in drag. The low Re results from WSU can be extended into the high Re results from F1 (at least over the range of M and Re shown) once the offset in the drag values between the two facilities is accounted for.

a) Maximum lift

b) Usable lift

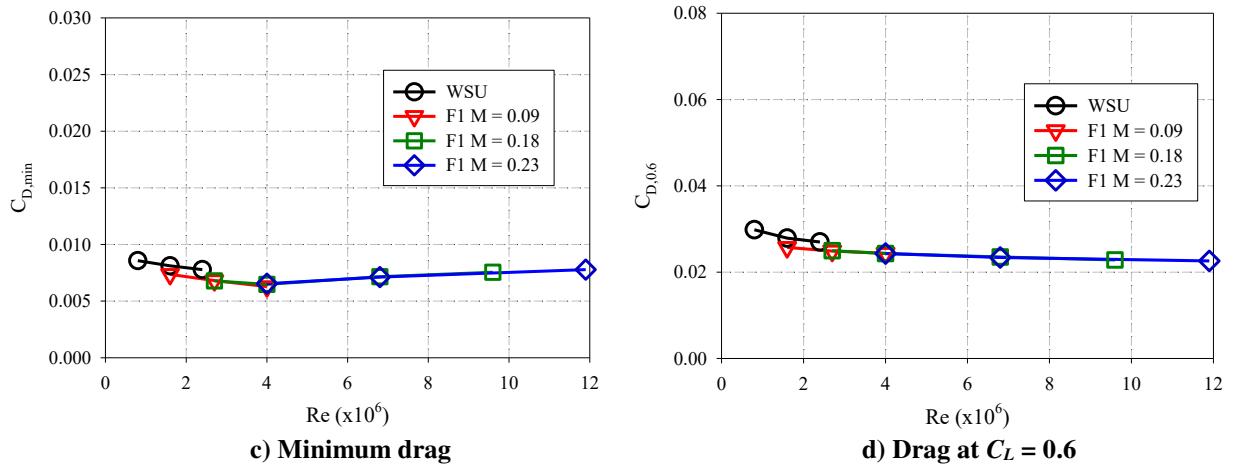**c) Minimum drag**

d) Drag at $C_L = 0.6$
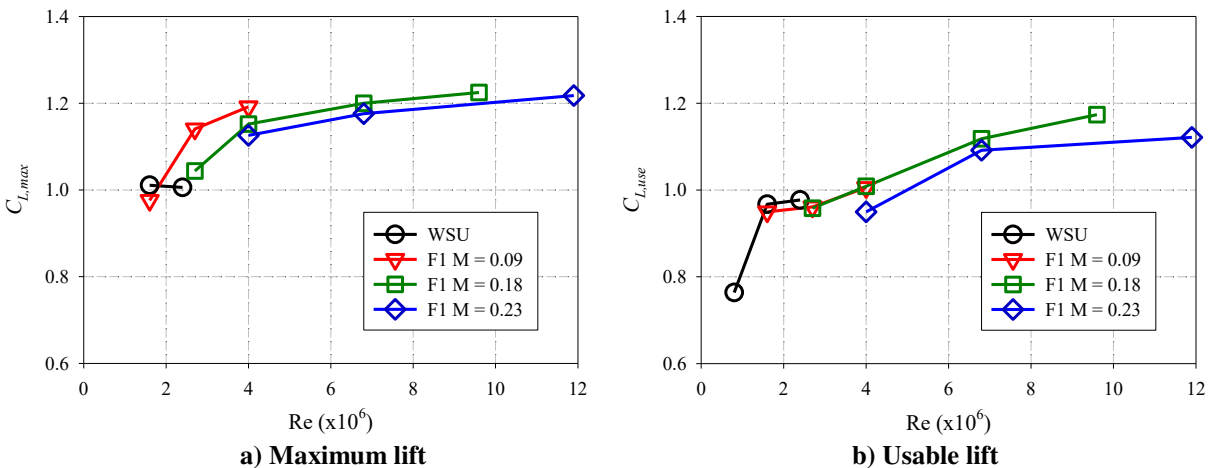
Figure 20. Clean model performance parameter comparisons.

Figure 21 shows the comparison of the performance parameters for the Maximum Scallop High Fidelity ice shape. This was the largest of the high fidelity ice shapes tested in this study and had the largest aerodynamic penalties. The comparison of $C_{L,max}$ is not shown because during the test at WSU, the data were not taken at sufficiently high enough angles of attack to capture the $C_{L,max}$ as traditionally described (Fig. 10). Figure 21a shows the comparison of the usable lift coefficient. The first thing to note is that the $C_{L,use}$ values for this ice shape was substantially lower than that of the clean wing, at roughly 60%, depending on the *Re* and *M* conditions. The values were also insensitive to *Re* and *M* effects in the F1 data. The WSU data show $C_{L,use}$ values similar to those from the F1 data, but show some variation with the Reynolds number. Some of this variation was thought to have been due to how the data were extracted. The $C_{L,use}$ values were obtained at angles of attack that corresponds to $C_{M,min}$. Figure 10 shows that for the Max Scallop High Fidelity ice shape, the $C_{M,min}$ values occurred in a region of relatively low gradient for C_M. This was compounded by the fact that for the WSU data, there was 1° between every angle of attack point, whereas in the F1 data, there was 0.5° between every angle of attack point. This increased the uncertainty in the angle of attack at which $C_{M,min}$ occurred (and the fact that the lift curve slope was still relatively high at this angle of attack) led to increased scatter in the WSU $C_{L,use}$ values. A more accurate angle of attack for $C_{M,min}$ was obtained by curve fitting the C_M plot in this region, and the $C_{L,use}$ values were obtained by interpolating the curve fitted angle of attack values. The results are shown in Fig. 21a as the "WSU Fit" curve. This resulted in reduced scatter in the WSU data that fit the trends shown in the F1 data better.

The comparisons of $C_{D,min}$ and $C_{D,0.6}$ with the Max Scallop High Fidelity ice shape are shown in Fig. 21b and Fig. 21c, respectively. As in the clean configuration, there was no Mach number effect in drag. However, the F1 data showed that there was a slight reduction in $C_{D,min}$ and $C_{D,0.6}$ with the Reynolds number starting at *Re* = 2.7x10^6. There was little *Re* effect between *Re* = 1.6x10^6 and 2.7x10^6. It was not certain if this break in the trend was real or due to the measurement uncertainties due to low dynamic pressures. The WSU data showed a larger *Re* sensitivity in the drag-based performance parameters. Also, there was an offset in the drag values between the WSU and F1 data.
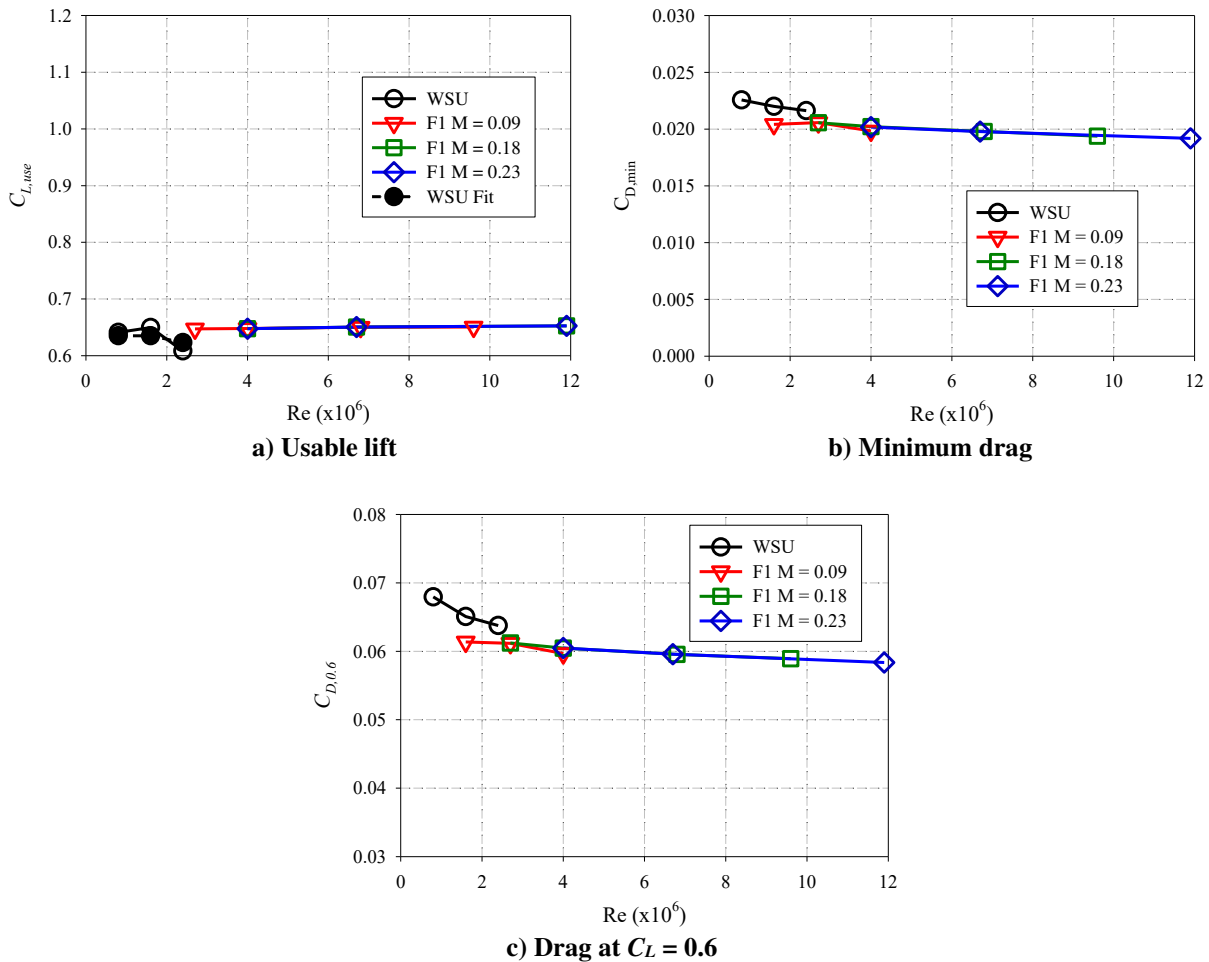
American Institute of Aeronautics and Astronautics

a) Usable lift

b) Minimum drag

c) Drag at $C_L = 0.6$

Figure 21. Max Scallop High Fidelity performance parameter comparison.

Figure 22 shows the comparison of the Streamwise 3D Smooth ice shape. This ice shape showed the highest level of Reynolds number sensitivity of the ice shapes tested in WSU and F1. Figure 22a shows the comparison of the maximum lift coefficient. There is no $C_{L,max}$ value shown for WSU test at $Re = 0.8x10^6$ because it was not present in the range of angles of attack that was tested. The figure shows that there was very little Mach number effect in the F1 data. There was also very little Reynolds number effect above $Re = 4x10^6$. Below $Re = 4x10^6$, there was substantial Reynolds number effect for both the WSU and F1 data. The WSU and F1 data agreed very well at matched Reynolds number. There was significantly more variation in the $C_{L,use}$ plots shown in Fig. 22b. In the F1 data, there was no Mach number effect between $M = 0.9$ and 0.18, but there were Mach number effects between $M = 0.18$ and 0.23. Interestingly, this was similar to what was observed for the clean case. The WSU data show a large change in $C_{L,use}$ value between $Re = 1.6x10^6$ and $2.7x10^6$. The $C_{L,use}$ value from WSU matched the F1 data well at $Re = 1.6x10^6$, but not at $Re = 2.4x10^6$. Figure 22c and 22d show the comparisons of the drag-based performance parameters. The trends shown here match very well with those from the Max Scallop High Fidelity case. There was no M effect, and slight Re effects. The WSU data showed the same trends as before, with an offset in the drag values when compared to the WSU data.

American Institute of Aeronautics and Astronautics

a) Maximum lift

b) Usable lift

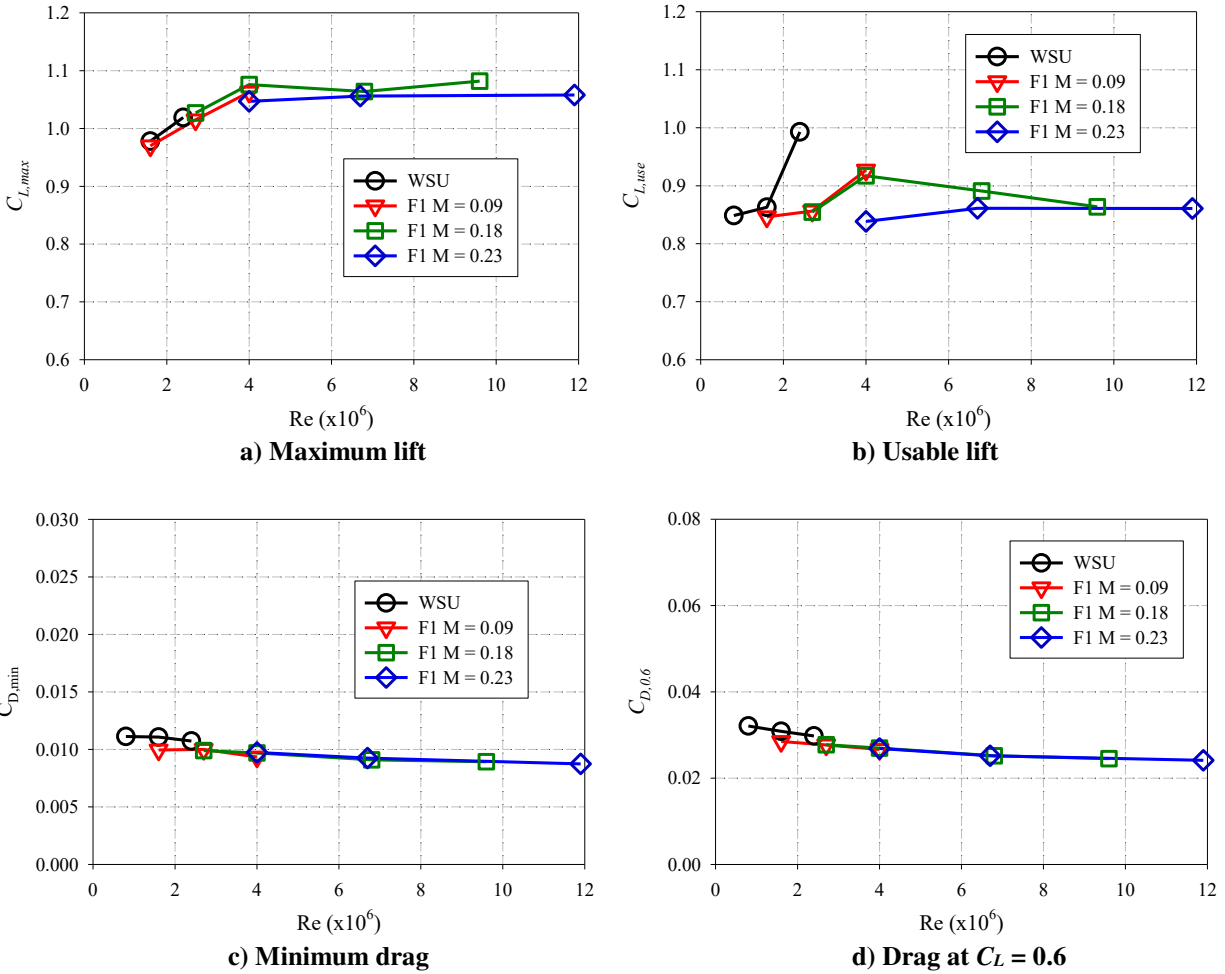**c) Minimum drag**

d) Drag at $C_L = 0.6$

Figure 22. Streamwise 3D Smooth performance parameter comparisons.

The comparison data for the two ice shape configurations showed that for iced configurations, the trends observed in the low Reynolds number (WSU test) could be extended to high Reynolds number (F1). In fact, for the high fidelity Max Scallop ice shape, the lift-based performance values can be used directly at high Reynolds number because there was no *Re* effect even down to *Re* tested in WSU. Broeren et al.[3] showed *Re* and *M* insensitivities for all high fidelity ice shapes that were test in F1. For more streamlined shapes such as the Streamwise 3D Smooth shape, one needs to be more careful on how the low *Re* results are used because there can be significant differences between low and high *Re* in lift-based parameters. In both ice shapes, there were *Re* effects in the drag-based parameters, so the trends for low *Re* can be applied to higher *Re*, but the values cannot be applied directly. Also, similar to what was observed for the clean configuration, the performance parameters obtained at WSU agreed well with those obtained at F1 at matched *Re* (and similar *M*).

IV. Conclusions

Artificial ice shapes of various geometric fidelity were tested on the CRM65 wing model. Low Reynolds number tests ($Re = 0.8 \times 10^6$ to 2.4×10^6) were conducted at Wichita State University's Beech Memorial Wind Tunnel, and high Reynolds number ($Re = 1.6 \times 10^6$ to 12×10^6) tests were conducted in ONERA's F1 wind tunnel. The aerodynamic performance data from the two facilities were compared at matched or similar Reynolds and Mach numbers to ensure that the low Reynolds number results from WSU could be applied to high Reynolds number.

Analysis of the clean wing data indicated that results from the low *Re* tests at WSU cannot be directly applied to high *Re* because of the Reynolds and Mach number effects. The clean wing data from the F1 tests clearly show both *Re* and *M* effects in the lift-based performance parameters. However, these effects could not readily be observed in the WSU data because *Re* and *M* could not be varied independently in the WSU tunnel (because it is an atmospheric tunnel). The drag-based performance parameters showed small *Re* effects and no Mach number effects in both facilities.

For iced configurations, the trends observed at low Reynolds number (WSU test) could be extended to high Reynolds number (F1). In fact, for the high fidelity Max Scallop ice shape, the lift-based performance values can be used directly at high Reynolds number because there was no *Re* or *M* effect. For more streamlined shapes, there can be measurable differences between low and high *Re* in lift-based parameters. As with the clean wing, there were *Re* effects in the drag-based parameters, so the trends for low *Re* can be applied to higher *Re*, but the values cannot be applied directly.

For both clean and iced configurations, the data from WSU and F1 agreed well at matched or similar *Re* and *M*. The lift and pitching moment curves agreed very well for most configurations. There appeared to be 0.2-0.3° offset in the angle of attack between the WSU and F1 data, possibly due to different flow angularities in the test sections of the two facilities. There was also an offset in the drag values between the two facilities from an unknown cause. Overall, the data compared very well between the low *Re* test at WSU and the high *Re* test at F1. This indicated that data from the low *Re* test could be used to understand iced-swept-wing aerodynamics at high *Re*.

Acknowledgements

References

[1] Broeren, A.P., Potapczuk, M.G., Riley, J.T., Villiedieu, P., Moens, F., and Bragg, M.B., "Swept-Wing Ice Accretion Characterization and Aerodynamics," AIAA Paper 2013-2824, June 2013, also NASA/TM—2013-216555, Sept. 2013.

[2] Vassberg, J.C., DeHann, M.A., Rivers, S.M., and Wahls, R.A., "Development of a Common Research Model for Applied CFD Validation Studies," AIAA Paper 2008-6919, Aug. 2008.

[3] Broeren, A.P., Potapczuk, M.G., Lee, S., Malone, A.M., Paul, B.P., Jr., and Woodard, B.S., "Ice-Accretion Test Results for Three Large-Scale Swept-Wing Models in the NASA Icing Research Tunnel," AIAA Paper 2016-3733, June 2016; also NASA/TM—2016-219137, Sept. 2016.

[4] Broeren, A.P., Addy, H.E., Jr., Bragg, M.B., Busch, G.T., Guffond, D., and Montreuil, E., "Aerodynamic Simulation of Ice Accretion on Airfoils," NASA/TP—2011-216929, June 2011.

[5] Morgan, H.L., Ferris, J.C., McGhee, R.J., "A Study of High-Lift Airfoils at High Reynolds Numbers in the Langley Low-Turbulence Pressure Tunnel," NASA TM-89125, 1987.

[6] Papadakis, M., Gile Laflin, B.E., Youssef, G.M, and Ratvasky, T.P., "Aerodynamic Scaling Experiments with Simulated Ice Accretions," AIAA 39th Aerospace Sciences Meeting and Exhibits, Jan. 8-11, 2001, Reno, NV, AIAA Paper 2001-0833.

[7] Addy, H.E, Broeren, A.P., Zoeckler, J.G., and Lee, S., "A Wind Tunnel Study of Icing Effects on a Business Jet Airfoil," AIAA 41st Aerospace Science Meeting and Exhibit, Jan. 6-9, 2003, Reno, NV, AIAA Paper 2003-0727.

[8] Lee, S., Ratvasky, T.P., Thacker, M., and Barnhart, B.P., "Geometry and Reynolds Number Scaling on an Iced Business Jet Wing," AIAA 43rd Aerospace Sciences Meeting and Exhibits, Jan. 10-13, 2005, Reno, NV, AIAA Paper 2005-1066, NASA TM-2005-213575.

[9] Woodard, B.S., Broeren, A.P., Diebold, J.M., and Bragg, M.B., "Preliminary Testing of Low Reynolds Number Aerodynamics for a Swept Wing with Artificial Ice Roughness," DOT/FAA/TC-17/48, Sept. 2017.

[10] Broeren, A.P., Lee, S., Woodard, B.S., Lum, C.W., and Smith, T.G., "Independent Effects of Reynolds and Mach Numbers on the Aerodynamics of an Iced Swept Wing," 10th AIAA Atmospheric and Space Environments Conference, Atlanta, June 2018 (submitted for publication), 2018.

[11] Broeren, A.P, Addy, H.E., Jr., Lee, S., Monastero, M.C., "Validation of 3-D Ice Accretion Measurement Methodology for Experimental Aerodynamic Simulation," NASA/TM—2015-218724, July 2015.

[12] Addy, H.E., Jr., Broeren, A.P., Zoeckler, J.G., and Lee, S., "A Wind Tunnel Study of Icing Effects on a Business Jet Airfoil," AIAA Paper 2003-0727, Jan. 2003; also NASA/TM—2003-212124, Feb. 2003.

[13] Pope, A., Rae, W. H., and Barlow, J.B. (1999). Low-Speed Wind Tunnel Testing (3rd ed.). Hoboken, NJ: John Wiley & Sons, Inc.

[14] "Data Reduction System: Boundary Corrections Three Dimensional Aircraft," Walter H. Beech Wind Tunnel Engineering Process Description, April 2014.

[15] Torz-Dupuis, L., "Test NASA SUNSET II of the CRM65 Wing Model Representative of the CRM65 Wing at 1/7.5 on Half Model Set-up in the ONERA F1 Wind Tunnel," ONERA Report No. PV 4/23611 DMPE/DSFM, Dec. 2017.

[16] Coleman, H.W., and Steele, W.G., *Experimentation and Uncertainty Analysis for Engineers*, Wiley-Interscience, New York, 1989, pp.40-118.

[17] Kline, S., and McClintock, F.A, "Describing Uncertainties in Single Sample Experiments," Mechanical Engineering, Vol. 75, No. 1, 1953, pp. 3-8.

[18] Camello, S. C., Lee, S., Lum, C. W., and Bragg, M. B., "Generation of Fullspan Leading-Edge 3D Ice Shapes for Swept-Wing Aerodynamic Testing," Proceedings of the 8th AIAA Atmospheric and Space Environments Conference, AIAA Paper 2016-3737, Washington D.C., June 2016.

[19] Federal Aviation Administration, Advisory Circular AC 25-25A, Oct. 27, 2014.

[20] Camello, S.C., Bragg, M.B., Broeren, A.P., Lum, C.W., Woodard, B.S., and Lee, S., "Effect of Ice-Shape Fidelity on Swept-Wing Aerodynamic Performance," AIAA Paper 2017-4373, June 2017.

[21] Broeren, A.P., Woodard, B.S., Diebold, J.M., and Moens, F., "Low-Reynolds Number Aerodynamics of an 8.9% Scale Semi span Swept Wing for Assessment of Icing Effects," 9th AIAA Atmospheric and Space Environments Conference, Denver, CO, 2017, AIAA Paper 2017-4372, NASA TM 2017-219533.

[22] Sandhu, N., Soltani, R., Bragg, M.B., Lum, C.W., Woodard, B.S., Broeren, A.P., and Lee, S., "Effect of Simulated Scalloped Ice on the Aerodynamics of a Swept-Wing at Low-Reynolds Number," AIAA 10th Atmospheric and Space Environments Conference, Atlanta, GA, June 25-29, 2018 (submitted for publication), 2018.

[23] Woodard, B.S., Broeren, A.P., Lee, S., Lum, C.W., and Bragg, M.B., "Summary of Ice Shape Geometric Fidelity Studies on an Iced Swept Wing," AIAA 10th Atmospheric and Space Environments Conference, Atlanta, GA, June 25-29, 2018 (submitted for publication), 2018.

[24] Glauert, H., "The Effect of Compressibility on the Lift of an Aerofoil," R. & M. No. 1135, British ARC, 1927.

[25] Furlong, G.C., and McHugh, J.G., "A Summary and Analysis of the Low-speed Longitudinal Characteristics of Swept Wings at High Reynolds Number, NACA-TR-1339, Jan. 1957.

[26] Lynch, F.T., and Khodadoust, A., "Effects of Ice Accretions on Aircraft Aerodynamics," *Progress in Aerospace Sciences*, Vol. 37, No. 8, Nov. 2001, pp. 669-767.